Characterization of mechanical properties and fracture mode of additively manufactured carbon fiber and glass fiber reinforced thermoplastics

Goh, Guo Dong; Dikshit, Vishwesh; Nagalingam, Arun Prasanth; Goh, Guo Liang; Agarwala, Shweta; Sing, Swee Leong; Wei, Jun; Yeong, Wai Yee

2017

Goh, G. D., Dikshit, V., Nagalingam, A. P., Goh, G. L., Agarwala, S., Sing, S. L., Wei, J. & Yeong, W. Y. (2017). Characterization of mechanical properties and fracture mode of additively manufactured carbon fiber and glass fiber reinforced thermoplastics. Materials and Design, 137, 79-89. https://dx.doi.org/10.1016/j.matdes.2017.10.021

https://hdl.handle.net/10356/82404

https://doi.org/10.1016/j.matdes.2017.10.021

This is an Authors' Original Manuscript (AOM); that is, the manuscript in its original and unrefereed form; a 'preprint' of an article published by Elsevier in Materials & Design on 5/01/2018, available online: https://doi.org/10.1016/j.matdes.2017.10.021.

Characterization of mechanical properties and fracture mode of additively manufactured carbon fiber and glass fiber reinforced thermoplastics

G. D. Goh[1], V. Dikshit[2], A. P. Nagalingam[2], G. L. Goh[1], S. Agarwala[1], S. L. Sing[1,2], J. Wei[3], W. Y. Yeong[1,2*]

[1]Singapore Centre for 3D Printing, Nanyang Technological University, 50 Nanyang Avenue, Singapore 639798

[2]School of Mechanical and Aerospace Engineering, Nanyang Technological University, 50 Nanyang Avenue, Singapore 639798

[3]Singapore Institute of Manufacturing Technology, 71 Nanyang Drive, Singapore 638075

*Corresponding Author

Designation: Assistant Professor, school of Mechanical and Aerospace Engineering, Nanyang Technological University, Singapore

Email: WYYeong@ntu.edu.sg

Tel: 67904343

Abstract

Continuous fiber-reinforced polymer (FRP) composites have been used for many applications to create strong yet lightweight products due to their high strength-to-weight and stiffness-to-weight ratios. Aerospace [1], automotive [2], and sport [3]industries are three of the few industries that have been using FRP composites. The increasing need for prototyping and customization of fiber reinforced polymer composite parts is prompting innovations in new manufacturing processes to realize short manufacturing cycle time and low production cost, which is challenging to accomplish using conventional molding process. Fused filament fabrication (FFF) -a material extrusion additive manufacturing (AM) technique trademarked as fused deposition modelling (FDM) by Stratasys- holds promise to achieve low-cost production on continuous fiber-reinforced thermoplastic (FRTP) composites. In this paper, the FFF technique is employed to fabricate continuous carbon and glass FRTP composites and its microstructural characteristics and the resulting tensile, flexural, and quasi-static indentation characteristics of the printed composites are examined. Additionally, the fracture behavior of each test sample is evaluated and discussed in detail.

Keywords: Carbon fibers, Polymer-matrix composites (PMCs), Mechanical testing, Microstructural analysis, 3-D printing, Additive manufacturing

1. Introduction

Additive manufacturing (AM) is a layer-by-layer manufacturing process in which parts are robotically manufactured from digital geometries [4]. It is a disruptive technology because it dramatically shortens the timeline for parts being designed and fabricated to end user requirements. Parts with intricate internal geometries such as honeycomb structure can be fabricated using AM which would otherwise be challenging or impossible using conventional techniques [5-7]. In polymer printing, many materials have been developed which are specific to the AM techniques employed [8]. For instance, thermoplastic polymer are developed for fused filament fabrication [9], powder materials for selective laser sintering [10] and liquid photopolymers for polyjet and stereolithography [11, 12]. However, the low mechanical properties that pure polymers typically exhibit are not suitable for high performance engineering applications. Recent trend shows the development of composite materials specifically for AM with enhanced mechanical properties over existing polymeric materials [13].

A composite material is a material made from two or more constituent materials with significantly different physical or chemical properties that, when combined, produce a material that offers superior overall performance compared to the individual components [14]. Research on development of composite materials for AM processes has been ongoing for more than a decade[15]. Most studies were focused on the development of materials with short fiber reinforcements [16-27] with only a few on continuous fiber reinforcements [28-38]. Although short fiber reinforced composites offer better mechanical performance compared to their unreinforced counterparts, there is still a substantial gap between the mechanical properties of additively manufactured composites and conventionally manufactured fiber reinforced polymer (FRP) composites, which mainly use continuous fiber reinforcement, in terms of mechanical

properties. For instance, the tensile strengths of additively manufactured short fiber composites are in the range of 70 MPa [16, 17, 39] which are inferior to the strengths of conventionally manufactured FRP's (200-1500 MPa) [40].

Although AM of composite material have been ongoing for the past decade, AM of continuous fiber reinforced thermoplastics (FRTP) composites are still in its infancy. To date, only stereolithography [28-30] and free form fabrication (FFF) [31-37] have been used to fabricate continuous fiber reinforced composites. FFF -a material extrusion AM technique- is seen to be the more promising technique compared to stereolithography to realize the fabrication of FRTP due to several reasons. Firstly, it is technologically less demanding and can be achieved with a slight modification on the extrusion print head. Secondly, the FFF feedstock materials have much longer shelf life as they are less susceptible to degradation.

In general, two methods have been developed for the FFF technique to realize the fabrication of FRTP composites, they are (1) in-situ fusion [31-36] and (2) extrusion of pre-impregnated fiber [41-44]. In in-situ fusion method, dry carbon fibers are fused with melted thermoplastics resins such as ABS and PLA in the FFF print head extruder. This method has the potential to create functionally graded composite parts by varying the amount of thermoplastic being extruded which in turn changes the fiber volume fraction. However, poor bonding at the fiber matrix interface resulting from the in-situ fusion remains one of the key challenges to be addressed [45]. On the other hand, although extrusion of pre-impregnated fiber (Fig. 1) does not give the flexibility to change the fiber volume fraction, it eliminates the problem of poor fiber matrix interface. This is because good impregnation can be performed with proper monitoring and quality control during the fabrication of pre-impregnated fibers. The fabrication of continuous fiber reinforced composites directly from pre-impregnated fiber has been attempted.

The MarkOne composite printer that uses extrusion technique to print continuous glass and carbon fibers has also been made available commercially giving product designers an alternative to realize their product design [46]. A detailed evaluation of mechanical properties of additively manufactured carbon fiber and glass fiber reinforced are very limited to the authors' knowledge.

Potentially, there is a need to characterize the mechanical properties and fracture behaviors of the additively manufactured continuous FRP composites to give product designers a detailed understanding on the characteristics of the additively manufactured continuous FRP composites. In this paper, the two types of commonly used fibers (carbon and glass fibers) are chosen to be evaluated due to their distinctly different raw material cost. Carbon fibers are known for their high stiffness-to-weight ratio but expensive ($150 per 50cm^3) and hence are only used in industries that are very particular about weight such as aerospace industry. On the other hand, glass fibers are relatively inexpensive ($75 per 50cm^3) and exhibit fairly good mechanical properties and are suitable for parts that are less stringent on weight and strength (especially for sports industry) so that parts can be fabricated at lower cost. Various mechanical properties that are relevant to sports, automotive, and aerospace industries, such as tensile, flexural, and indentation resistance of additively manufactured continuous carbon and glass FRTP are evaluated by conducting mechanical testing. In addition to that, scanning electron microscopy (SEM) and micro-computerized tomography (μCT) -scan were also used to observed the microstructures and fracture mechanism of the composites.

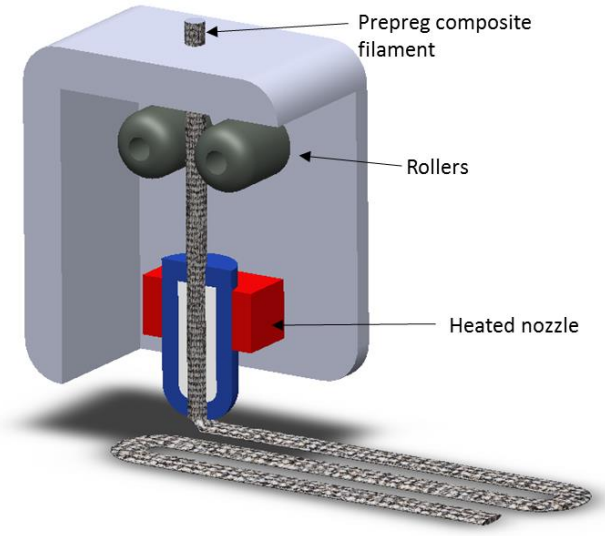

Figure 1 Extrusion of pre-impregnated continuous fiber composite filament in FFF

2. Material and test methods

2.1 Manufacturing process

The carbon and glass fibers are provided by Markforged, United States. The materials are composed of multiple strands of carbon or glass fibers coated with nylon matrix and come in spools [47]. The diameter and density of the carbon fiber composite filament were measured to be 370 microns and 1.30 g/cm^3. Similarly, the diameter and density of the glass fiber composite filament were measured to be 290 microns and 1.45 g/cm^3. The extruder temperature was set to 260 °C. The parts were fabricated with unidirectional pattern (0°) as shown in Fig. 2. Layer height was set as 0.1 mm. Air gap was kept zero to ensure the specimens were solid. Table 1 illustrates the parameters selected for part fabrication.

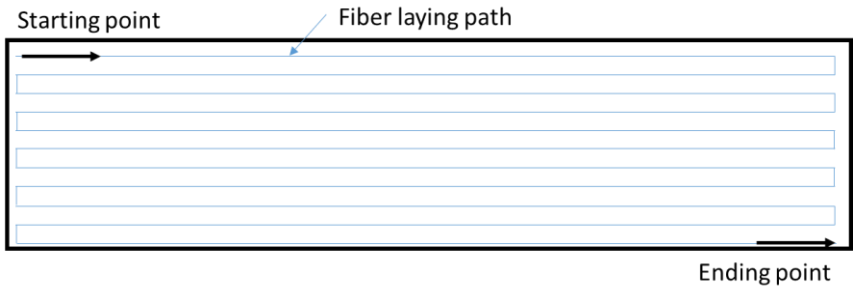

Figure 2 Isotropic unidirectional fiber pattern (0°) of a single layer. Fiber layers are stacked up on top of each other without any nesting.

Table 1 Printing parameters

Extruder temperature (°C)	Print pattern	Layer height (mm)	Infill (%)
260	Unidirectional	0.1	100 (solid)

2.2 Experimental methods

Microstructure analysis

After the tests, µCT-scan (Skyscan 1173, Bruker Co., United States) images of the fractured specimen were taken to observe the fracture mode and determine the porosity. The µCT-scan machine has a CCD sensor with 2240x2240 pixels, each with the pixel size of 50 µm. 1x1

camera binning mode was used and the resulting image pixel size was 16.404 μm when the object was placed 119.318 mm from the source. Source voltage, source current and the exposure time were set to 40 kV, 200 μA, and 1200 ms respectively. To investigate the interfacial and inter-layer properties of the continuous FRTP, the microstructure of the additive manufactured FRTP was observed using optical stereo microscope (SZX7, Olympus Co. Japan), laser scanning confocal microscope (VK-X250, Keyence, Japan) and SEM (JSM-IT300LV, JEOL (Japan Electro Optics, Ltd.), Japan).

Density, fiber content, and porosity measurements

The densities of the dry carbon fiber, pure nylon, and the composite materials were determined using Metler Toledo XS204 analytical balance. The fiber loading, V_f and the porosity were determined in accordance to the ASTM D3171-15 (Standard Test Methods for Constituent Content of Composite Materials) [48]. Burn-off technique was used to remove the matrix material. The material was heated linearly at the rate of 20 ^oC/min from room temperature to 500 ^oC to remove the matrix material.

Tensile test

The tensile test specimens were designed and printed according to ASTM D3039/D3039M-14 (Standard Test Method for Tensile Properties of Polymer Matrix Composite Materials) [49]. The dimension of the specimen is 25 x 250 x 2.5 mm. Three specimens are prepared for each type of fiber. The 23 layers of fibers were laid unidirectionally in 0°. Tensile test was conducted with a universal testing machine (100kN, Shimadzu Co., Japan). The crosshead speed was set to be 1.5 mm/min.

Flexural test

The flexural test specimens were designed and printed according to ASTM D790-15e2 (Standard Test Methods for Flexural Properties of Unreinforced and Reinforced Plastics and Electrical Insulating Materials) [50]. The dimension of the specimen is set to be 13 x 154 x 4 mm such that the support span-to-depth ratio is 32:1. The support span was set to be 128 mm. Three specimens are prepared for each type of fiber. The fiber was laid unidirectionally in 0°.

Flexural test was conducted with a universal testing machine 10kN, Shimadzu Co (10kN, Shimadzu Co., Japan). The loading and supports noses have a diameter of 5 mm. The crosshead speed was set to be 6.82 mm/min such that the strain rate is 0.01 mm/mm.min.

Quasi-static Indentation test

Indentation test specimens were designed and printed according to ASTM D6264/D6264M-12(Standard Test Method for Measuring the Damage Resistance of a Fiber-Reinforced Polymer-Matrix Composite to a Concentrated Quasi-Static Indentation Force) [51] with slight modification in specimens' dimensions. The dimension of the specimens is 100 x 100 x 1.6 mm. Three specimens are prepared for each type of fiber. Quasi-isotropic fiber layup was used in which fiber direction is changed by 45° from one layer to the next [0/45/90/-45] for 14 layers. Quasi-static indentation tests were conducted with a universal testing machine (10kN, Shimadzu Co., Japan). Standard indenter geometry which has a blunt, hemispherical tip with diameter of 13 mm was used. The specimens were tested in an edge supported condition (circular boundary with diameter of 78 mm) so that the deflection of the specimen and stiffness effect can be considered [5]. The test specimens were supported over a circular opening. Crosshead speed was 1.25 mm/min. The maximum indentation energy during quasi-static indentation was defined as the area under the loading curve.

3. Results and Discussion

3.1 Microstructure Analysis

This section discusses the effect of extrusion on the microstructures of the filament and additively manufactured composite parts. SEM images of the pre-extruded and extruded composite filament were taken in order to investigate the change in shape after the extrusion process. Both the pre-extruded and extruded composite filaments were broken at room temperature to capture the SEM images of the cross-section of the filaments. As shown in Fig.

3(a), the composite filament consists of multiple strands of continuous fibers coated with matrix. Figure 3(b) shows a composite filament before undergoing extrusion whereas Fig. 3(c) shows a composite filament after extrusion. The initial diameter of the composite filament is 460 µm. It is observed that the composite filament is flattened to 180 µm, after the extrusion process. Due to the flattening nature, the base is considerably wide (1.0 mm) making it impossible to create thin wall structures. Adjacent filaments are connected by partial overlapping (~ 250 µm) at the sides of the filament (Fig. 3(c)).

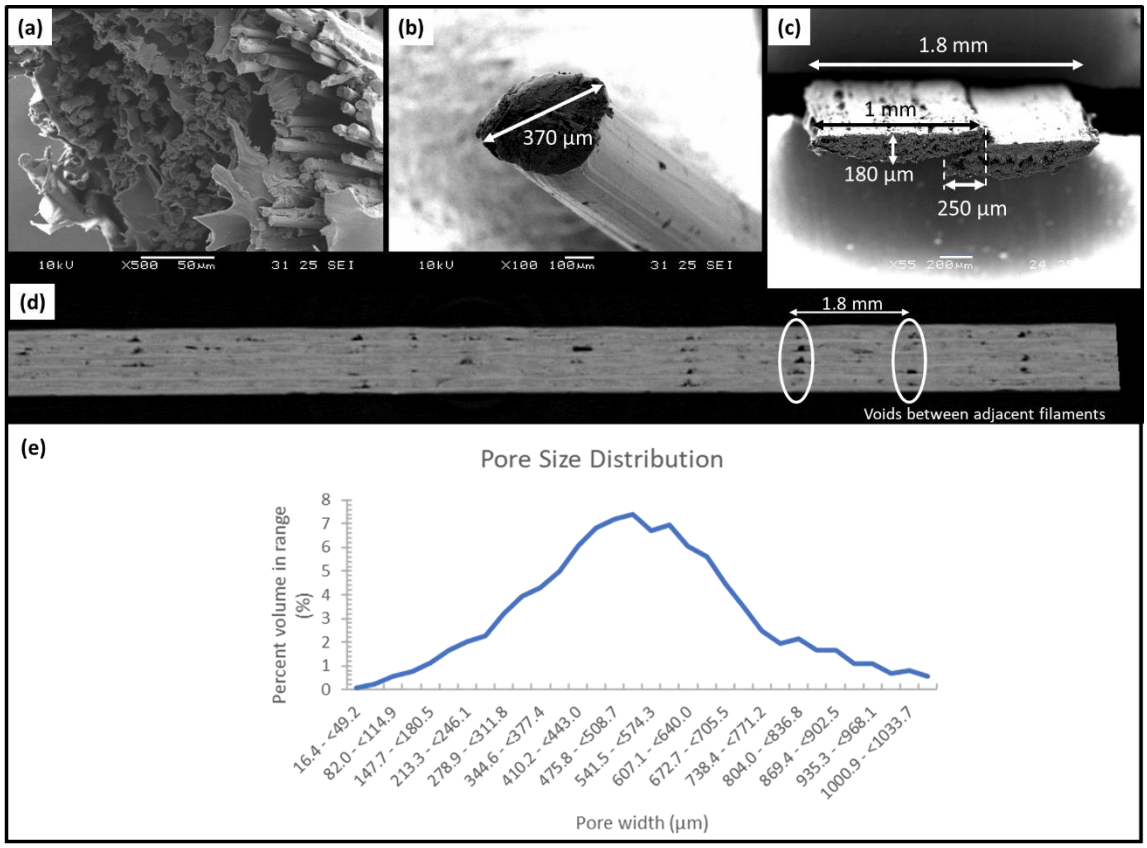

Figure 3(a) SEM image of composite filament showing multi-strands of fibers (b) SEM image of a single raw carbon fiber composite filament (c) SEM image of the two overlapping extruded composite filaments (d) CT-scan image of cross section of composite specimen showing the voids formed between adjacent filament (e) Pore size distribution obtained from µCT-scan analysis

The fiber matrix interface of the extruded carbon fiber composite filament can be observed in Fig. 3(a). It is observed that there are voids in several regions of the extruded filament. This could be due to improper impregnation of nylon matrix during the fabrication of carbon fiber composite filament. Another reason could be the lack of consolidation process to enhance the fiber-matrix bonding and to reduce porosity. The porosity of the additively manufactured CFRTP are determined using μCT-scan and density calculation method. In μCT-scan, the porosity is calculated as the percentage of ratio of the voids area (black area within the cross section of the specimen) to the cross-sectional area. The pore size distribution from the μCT-scan analysis is shown in Fig. 4 and the average porosity is found to be 2.7%. It should be noted that the porosity obtained from μCT-scan analysis is most likely underestimated as pores smaller than pixel size (16.4 μm) will not be detected. From (Fig. 3(d)), the μCT-scan is able to capture the voids between the adjacent filament, which are normally larger than 16.4 μm. However, the density calculation method reveals that the porosity of the extruded composite is about 10%, which is much higher than the 2.7% obtained from μCT-scan analysis. This suggests that micro pores with size smaller than 16.4 μm exist in the extruded filament and constitutes most of the porosity in the extruded composite materials.

To investigate the laying of the continuous carbon fibers composite filament, the printed carbon fiber parts were put under the optical stereo microscope and laser scanning confocal microsope to observe if there is any discontinuity of fibers along the laying direction. Figure 4(a) shows an optical image and figure 4 (c), and (d) show high magnification laser-optical images of the extruded carbon fibers. It is observed that there is no obvious crack indicating the carbon fiber is still continuous. However, it is unclear whether the carbon fibers have some micro cracks formed due to the perpendicular laying which might affect the mechanical properties of the printed parts and could not be observed using the laser scanning confocal microscope and the μCT-scanner. Future study to investigate the effect of laying direction on the formation of micro cracks and thus the mechanical properties is being considered.

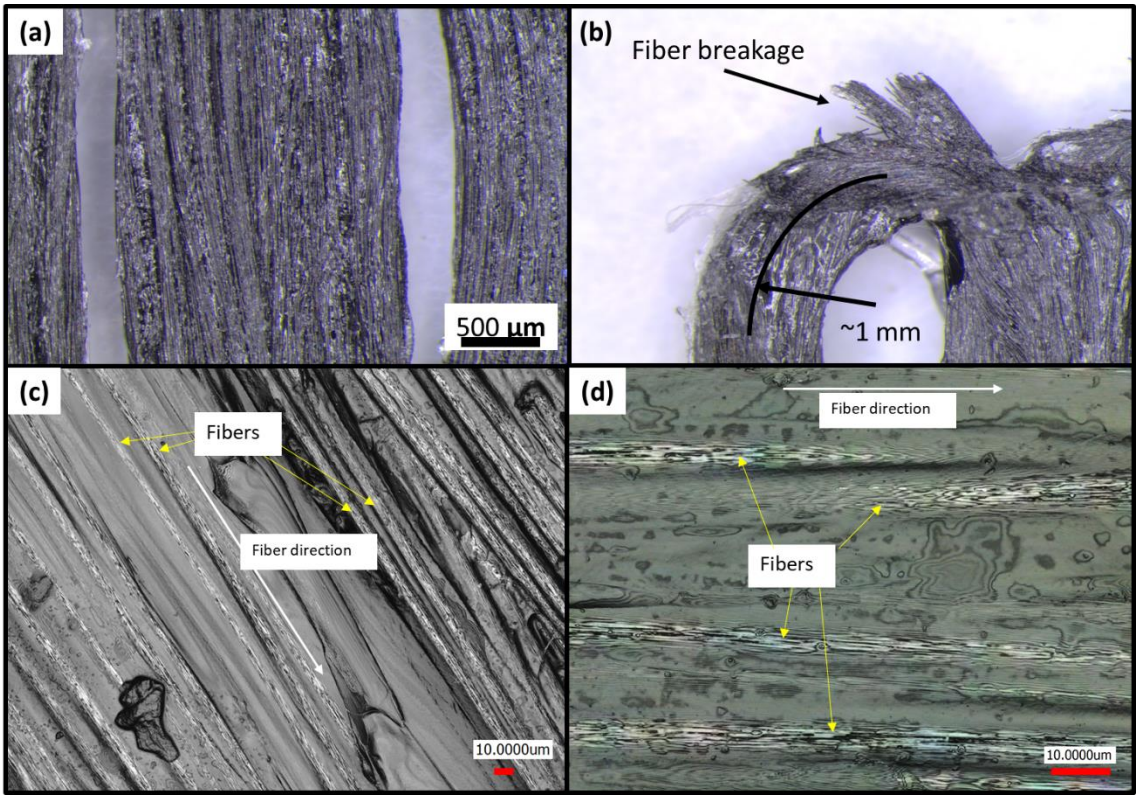

Figure 4 (a) continuous carbon fiber without observable breaking under optical microscope (b) breaking of carbon fibers at small turn radius (c) laser-optical image of multiple-strands of fibers at 50x magnification (d) laser-optical image of multiple-strands of fibers at 150x magnification

In addition, the design window of the laying of the carbon fibers is investigated. A single-layer benchmark part with various turning radii (1, 1.5, 2, 2.5 and 3 mm) was printed and put under the optical microscope to observe the microstructures of the printed part. Carbon fiber breakage was observed for turning radii approximately 1 mm (Fig. 4(b)).

3.2 Mechanical properties

In this section, the tensile, flexural, and indentation resistance properties of the additive manufactured carbon fiber reinforced thermoplastic (CFRTP) and glass fiber reinforced thermoplastic (GFRTP). Three specimens were tested per material for each type of test. A comparison of the mechanical properties between carbon and glass FRP is shown in table 2. It should be noted that the fiber volume fraction of carbon fiber (41 $_{vol}$%) is slightly higher than that of the glass fiber (35 $_{vol}$%). The failure mode of each test is also observed and evaluated.

The larger discrepancy of the young's modulus and the flexural modulus from the manufacturer's data could be due to difference in method in obtaining the strain values. Data for conventional carbon and glass fiber reinforced composites are shown to serve as references.

Table 2 Mechanical properties of FFF-fabricated CFRTP and GFRTP (average value ± standard deviation).

		FFF GFRTP (V_f: 35_{vol}%)	Manufac-turer's data (GFRTP)	Conven-tional glass fiber composites	FFF CFRTP (V_f: 41_{vol}%)	Manufac-turer's data (CFRTP)	Conven-tional carbon fiber composites
Tensile test	Tensile Strength (MPa)	450 ± 1	590	225-235 [a]	600 ± 30	700	408[b]
	Young's Modulus (GPa)	7.20 ± 0.01	20	16.9-17.9 [a]	13.0 ± 1.0	50	71.4 [b]
Flexural test	Flexural Strength (MPa)	149± 10	310	356-359 [a]	430 ± 13	470	750[c]
	Flexural Modulus (GPa)	14.7±0.5	21	15-15.4 [a]	38.1 ± 1.0	48	47 [c]
Quasi-static Indentation test	Maximum Force, F_{max} (N)	1410 ±108	NA	NA	1080 ± 123	NA	1580[d]
	Displace-ment at maximum force (mm)	7.68 ± 0.43	NA	NA	3.54 ± 0.20	NA	NA
	Displace-ment @ 0.2*F_{max} (mm)	13.0 ± 1.0	NA	NA	10.6 ± 0.3	NA	NA
	Maximum Energy (J)	7050 ± 268	NA	NA	6260 ± 668	NA	NA

[a] V_f=38.3~41.5% E-glass stitched multi-axial non-crimp fabrics/epoxy composites[40]
[b] V_f=40% unidirectional carbon fabric/ PA 6/6 composites [52]
[c] V_f=47.5% unidirectional carbon fiber/epoxy composites [53]
[d] CFRP with a 0/90 configuration[54]

3.1.1 Tensile properties

Figure 5(a) shows a typical tensile stress vs strain graph of the additively manufactured carbon fiber and glass fiber tensile coupons. For both carbon fiber and glass fiber, it is observed that the stress increased almost linearly with the strain before breaking abruptly at 5.2% and 6.2% strain for carbon and glass fibers respectively, indicating brittle nature of the composite. The

maximum tensile strength and Young's modulus recorded for carbon fiber samples was 600 MPa and 12.99 GPa respectively whereas the maximum tensile strength and Young's modulus recorded for glass fiber was 450 MPa and 7.20 GPa respectively. The longer elongation before rupture for glass fibers indicates that glass fibers are more flexible than carbon fibers. A drop in slope is noticed in stress-strain curves of both materials. Similar results have been obtained by Li *et al.* [31]. The sudden drop in tensile strength followed by a slight rise before a complete failure was observed in all carbon fiber samples and it was likely due to localised fiber failure.

Figure 5(b) and (c) show the fracture mode of the additively manufactured carbon and glass fiber reinforced tensile coupon respectively. Figure 5(d) illustrates failure mechanisms occurred in the tensile specimen in the tensile test. Tensile rupture and shear rupture are observed in all the CFRTP and GFRTP specimens. Shear rupture is regarded as shear damage along the fiber direction whereas tensile rupture is regarded as damage in perpendicular to the loading direction. Horizontal cracks formed without necking as shown in Fig. 5(e) is the result of tensile rupture, which indicates the brittle nature of the composite. Additionally, specimens of both materials showed severe delamination after the tensile test. Also, de-bonding between two adjacent fiber filaments in the same layer is also noticed (Fig. 5(b) and (c)). Delamination and de-bonding (as observed in Fig. 5(e)) are the results of shear rupture. As the fiber layers and the fiber bundles are held together by the matrix, the delamination and de-bonding between fiber bundles indicate that weak bonding exists between the layers. The weak bonding between layers is attributed to the lack of consolidation process in the FFF technique.

The micro-scale fracture mechanism can be observed using SEM. Large amount of fiber breakage is observed in Fig. 5(f) and (g). Extensive fiber breakage suggests that the failure mode of additively manufactured CFRTP and GFRTP specimens subjected to tension are fiber dominant, indicating loads are effectively transferred from matrix to fibers. Figure 5(g) shows that matrix adheres onto the fiber which indicates good interfacial bonding between matrix and fiber. Although the printed composite part generally has a good fiber-matrix interfacial bonding, a small number of holes observed (Fig. 5(f)) suggests that only a very small amount fiber pull-

out occurred in the tensile test. The small amount of pull-out could be due to the improper coating of nylon matrix onto the fiber surface during the fabrication of composite filament. That said, the fiber pull-out is generally insignificant in comparison to the large number of fiber breakage.

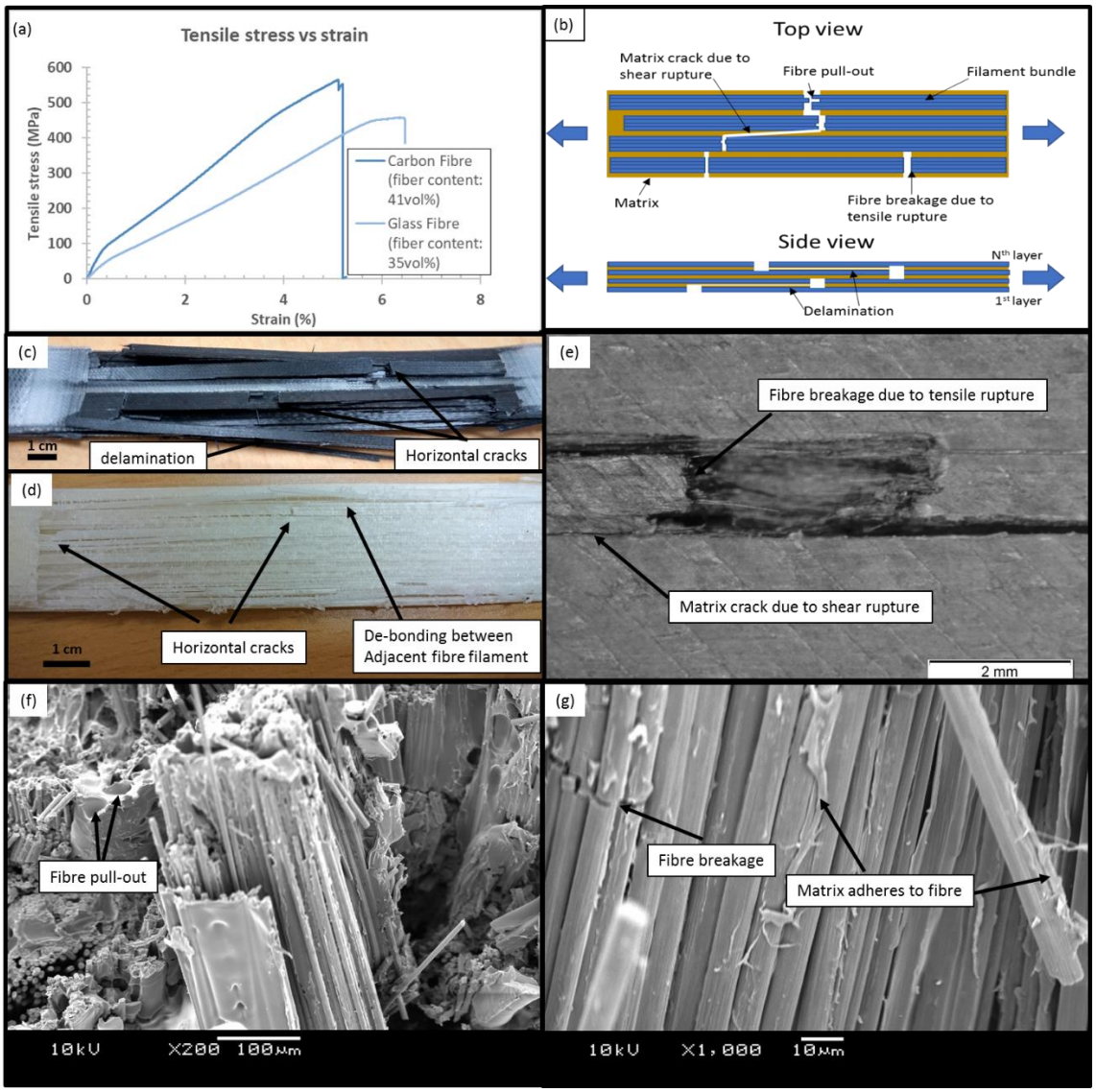

Figure 5 (a) Stress-strain curves of an additively manufactured carbon and glass FRTP (b) illustration of tensile fracture mechanism of additively manufactured FRTP (c) fracture mode that consists of cracking and delamination of a carbon fiber tensile specimen (d) fracture mode that consists of cracking and delamination of a glass fiber tensile specimen (e) matrix crack due to shear rupture and fiber breakage due to tensile rupture (f) SEM image showing fiber pull-out at the fractured surface (g) SEM image showing fiber breakage and matrix adhering to fiber

3.1.2 Flexural properties

For both carbon and glass fibers, the flexural stress is linear up to 1.0% flexural strain (Fig. 6). At 1.0% strain, a slight drop in flexural stress is observed. Different trends are observed after the slight drop at 1.0% strain. For carbon fiber, the reason for the drop could be due to localised fiber breakage on the tensile side of the specimen. The flexural stress continues to rise after the slight drop. The flexural specimens broke abruptly upon reaching the maximum flexural strength with corresponding strain of 1.5%. The maximum flexural strength and flexural modulus recorded for carbon fiber were 430 MPa and 38.1 GPa respectively. For glass fiber, the flexural stress continues to rise gradually until it reaches a maximum point before gradually decreasing after 2.5% strain. No sudden rupture is observed for glass fiber specimen. The maximum flexural strength and flexural modulus recorded for glass fiber were 149 MPa and 14.7 GPa respectively, around 40% of the strength and modulus of carbon fiber.

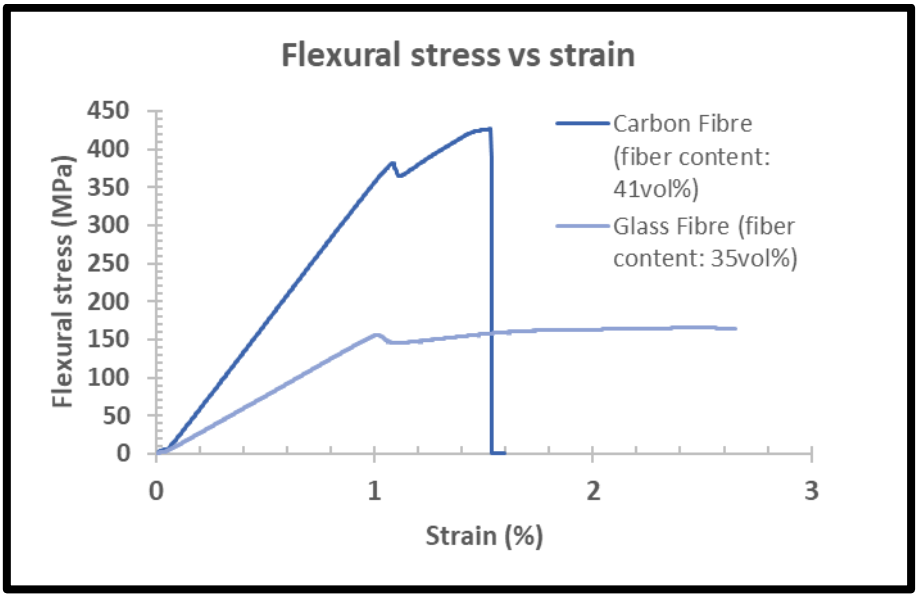

Figure 6 Typical 3-point bending test response of AM carbon and glass FRTP composite specimens

In fracture analysis of carbon fiber specimens, a high-speed camera (Fastcam SA4, Photron, Japan) was used to observe the fracture mechanism of the carbon fiber specimens at 5000 frames per second. Crack initiation at the top-most surface of the compression side was first

observed (Fig. 7 (d-ii)). The crack was likely formed as a result of crushing of fibers due to the high compressive stress at the top-most surface. The crack continued to propagate towards the neutral axis while the specimen still remained in one piece under the bending load (Fig. 7 (d-iii)). This behavior is similar to most of the conventional CFRP in which failure in compression is normally observed due to poor compressive strength of carbon fibers [55, 56]. The sudden drop in flexural stress at 1.57% strain is because the flexural specimens fail catastrophically when the fibers at the tensile side break. When the outermost fiber layers at the tensile side break (Fig. 7 (d-iv)), the bending load will have to be distributed among the remaining intact layers. However, the fewer number of layers that remains intact will not be able to take up more loads and would break eventually causing the catastrophic failure Fig. 7 (d-v)).

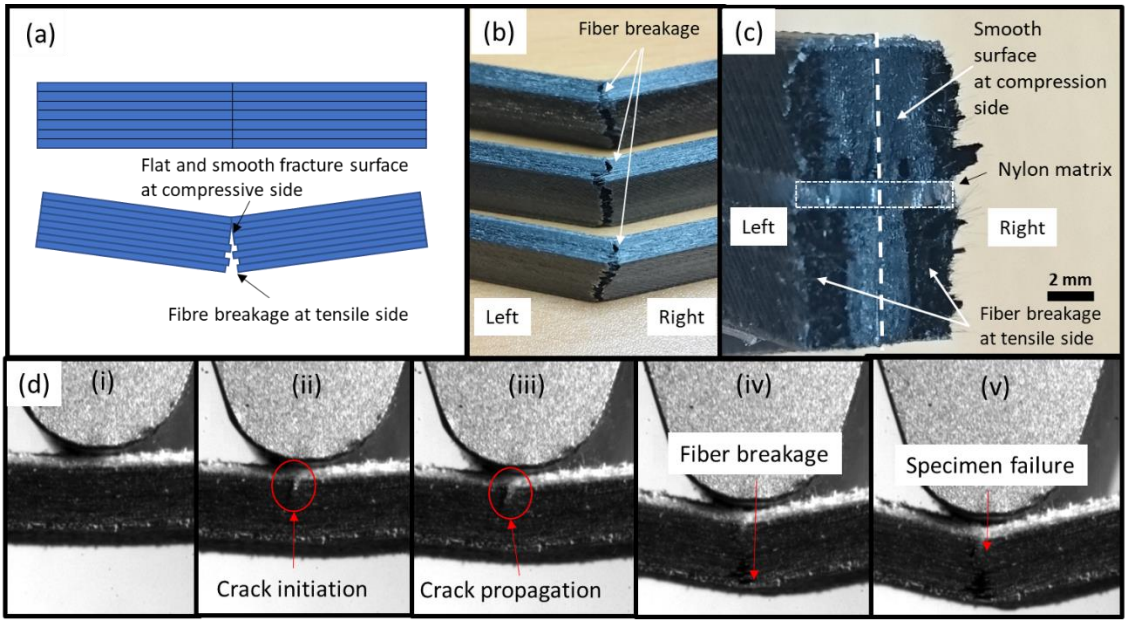

Figure 7(a) schematics illustrating fracture mode of carbon FRTP undergone flexural test (b) fibers breakage occurred at the outer most layers which are in tensile (c) cross section view of the fracture surface (d) image sequence of the flexural test captured using high speed camera

On the contrary, glass fiber specimens do not show failure in tension but rather buckling of fibers at the compression layers as illustrated in Fig. 8(a). The gradual decrease of flexural strength instead of an abrupt one can be explained from the fracture analysis. This is because the specimens do not fail in tension but rather it is just localised buckling at the compression layers

(Fig. 8(d)). Fiber buckling is likely due to the failure of the fibers as a result of shear kinking and matrix failure. The fracture mechanism of the glass fiber flexural test specimen is an example of a classical compression kink band in a composite material. The individual layers in the specimen are behaving as they should. However, the whole specimen is not behaving as a composite material, rather a composite structure, with poor bonding between adjacent filaments. De-bonding between two adjacent fiber filaments in the same layer is also noticed (Fig. 8(b)). The de-bonding is a result of shear kinking which introduces lateral force that separates the adjacent filament (Fig. 8(c)). The de-bonding between two adjacent fiber is also an indication of poor bonding between the fiber filaments. A closer inspection on the specimen reveals that shear kinking only happens in compressive layers as shown in Fig. 9(a), (b), (c), (d). In Fig. 9(b), de-bonding of adjacent filament is observed at the top layers which are in compression. No shear kinking is observed in the bottom layers which are in tension (Fig. 9(d)).

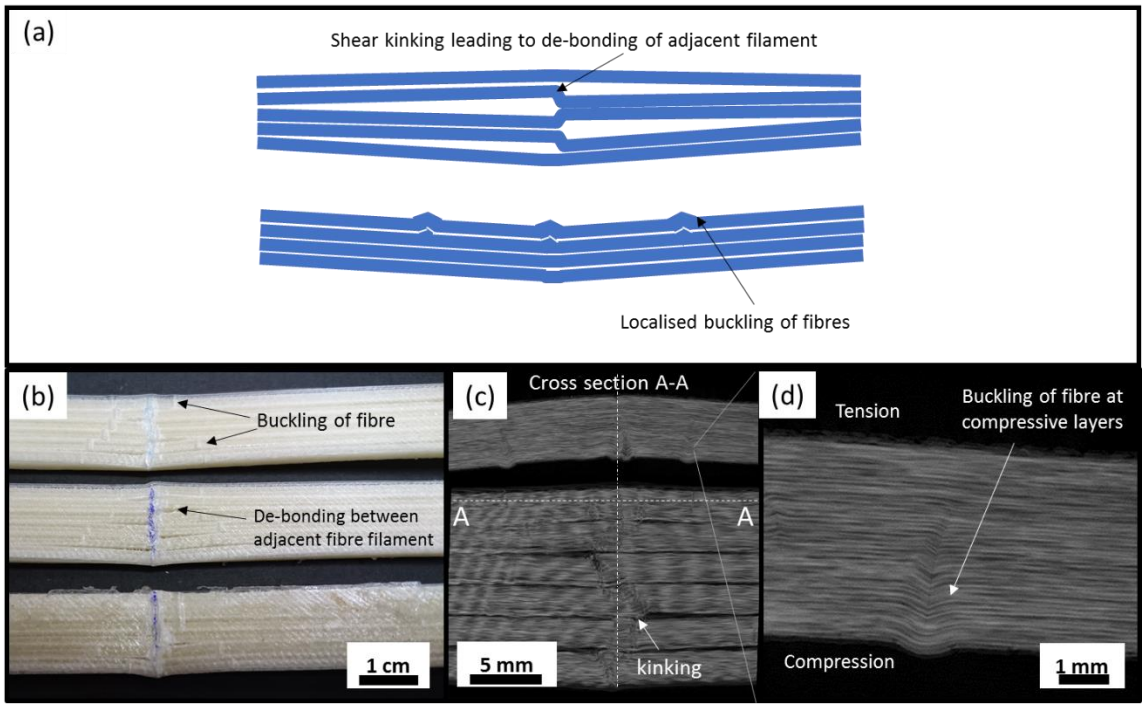

Figure 8 (a) schematic showing the fracture modes of the additive manufactured glass FRTP undergone flexural test (b) top view of glass fibers specimens with buckling of fibers (c) μCT image of the top view of the glass fibers specimen showing the shear kinking at the middle of the specimen (d) μCT image of the side view of glass fibers specimens showing the buckling of fibers at compressive layers

In short, good flexural data are hard to obtain from these AM glass fiber specimens, because they are not acting like proper composite materials due to poor bonding between adjacent filaments. One of the probable reason for the de-bonding of adjacent filament could be due to the difference in the diameter of the filaments, with glass fiber filament being 80 microns smaller than the carbon fiber filament. By using the same printing parameters, the glass fiber filament with the smaller diameter will result in lesser overlapping area which would result in poorer bonding between adjacent filament (Fig. 9(b)).

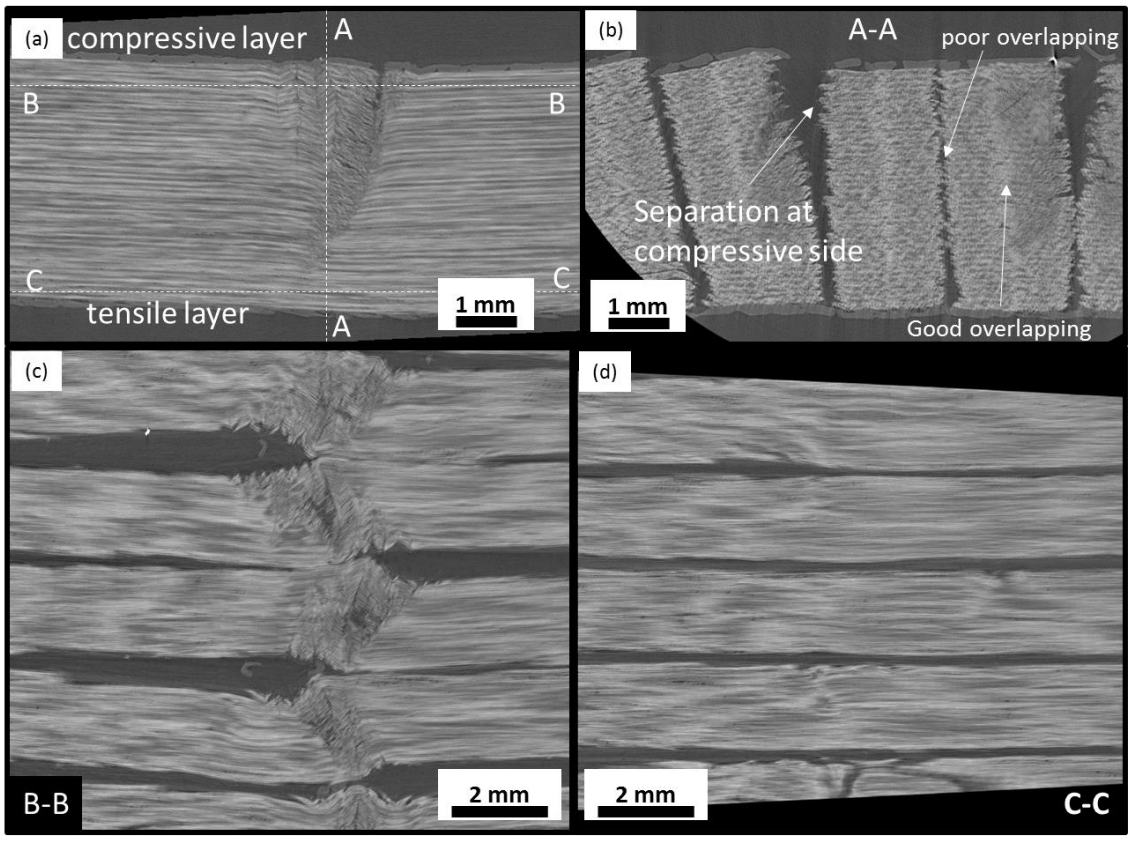

Figure 9 (a) μCT image of the side view of the glass fiber flexural test specimen undergone flexural test (b) cross sectional view of A-A (c) cut-out view of B-B showing shear kinking at top layer caused by poor bonding between adjacent filaments (d) cut-out view of C-C showing no obvious shear kinking at bottom layer

3.1.3 Indentation test

Figure 10 shows the typical results of the indentation test for carbon and glass fiber specimens. For carbon fiber, the indentation force increases to a maximum before dropping abruptly at 3.8

mm indentation when the quasi-isotropic carbon fiber sheet breaks. The force continues to rise initially after the sudden drop until a local maximum and begins to drop thereafter. The maximum indentation force recorded for the carbon fiber specimens was 1078 N and the indentation energy calculated up to 10.62 mm displacement (20% maximum force) was 6530 J. The sudden drop in indentation force is very similar to what happened in flexural test and could be due to the catastrophic failure at the tensile side of the carbon fiber flexural specimens.

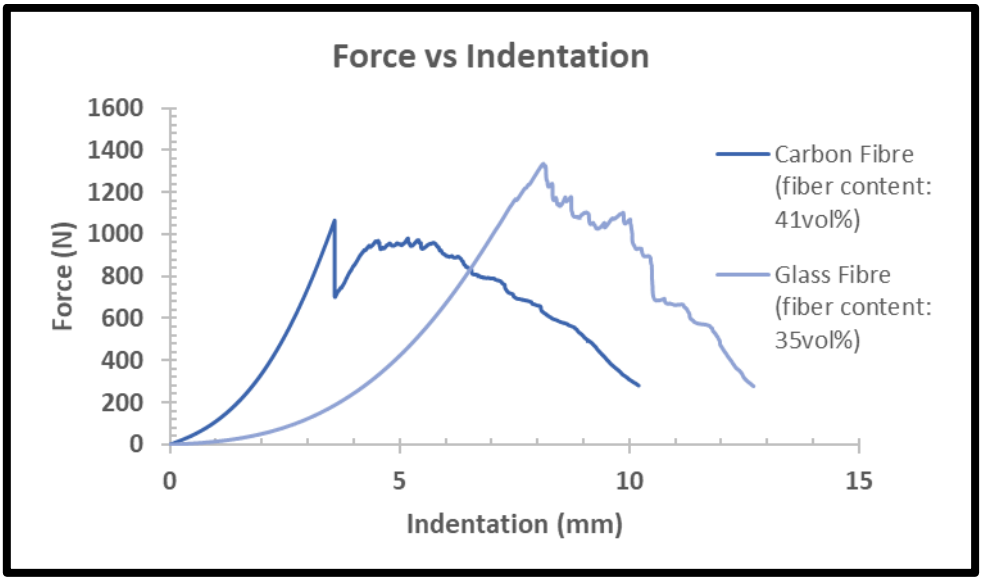

Figure 10 force-indentation curves for carbon and glass FRTPs

For glass fiber, the indentation force increases to a maximum before dropping gradually at 7.68 mm indentation when the quasi-isotropic glass fiber sheets break. The larger indentation at maximum indentation force of glass fiber is due to the lower Young's modulus and flexural modulus as compared to the carbon fiber. The maximum indentation force and the indentation energy calculated up to 12.12 mm displacement (20% maximum force) recorded for the glass fiber specimens was 1406 N and 7046 J respectively. This suggests that glass fiber has higher indentation resistance as compared to carbon fiber.

The typical fracture mode of additively manufactured carbon and glass fiber specimens is similar and the illustrations are shown in Fig. 11. During the test, a dent at the top layers is first observed and followed by fiber breakages at the bottom layers and eventually in all layers as the

indenter perforates the specimens (Fig. 11(a)). Delamination will also occur as a result of indentation.

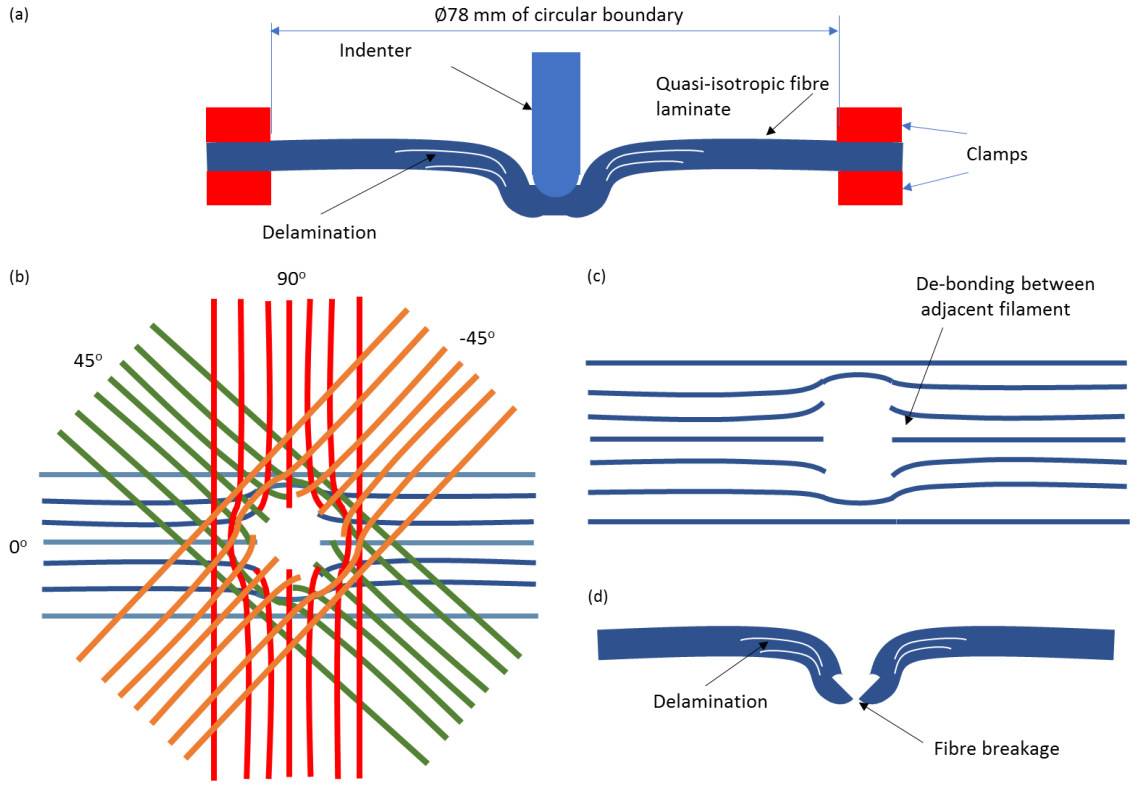

Figure 11(a) Deformation and delamination of fiber laminate before fiber breakage (b) fiber breakage of different fiber layup orientation after the indentation (c) failure mode of single fiber layup orientation which consists of fiber breakage and de-bonding between adjacent filament (d) cross section view which consists of delamination and fiber breakage in the indentation specimen

The fractured area is evaluated after the test. As noted earlier, the failure mode for carbon FRP (Fig. 12(a), (b)) is similar to glass FRP (Fig. 13(a), (b), (c)). No fiber breakage or delamination occurred in region far away from the indentation centre (Fig. 12(a-i)). Voids observed in Fig. 12(a-i) are results of the extrusion based fabrication method. Fiber breakage is observed at the middle where the indenter acted on and the maximum damage diameter (viewed from outside without considering internal damage) was 21 mm (Fig. 12(a-iii)). The average damaged area is found to be 201.5 mm^2 or 4.4% of the total area. In addition to that, delamination is observed

around the perforated region (Fig. 12(a-iii) for carbon FRP and Fig. 13(b), (c-ii) for glass FRP) and beyond the perforated region (Fig. 12(a-ii), (a-iv) for carbon FRP and Fig. 13(c-i) for glass FRP) in which black gaps between the layers are observed. This suggests that the delamination would propagate from the middle where indenter is acting on towards the side of the specimen and the affected area is often larger than the damaged area observed from outside.

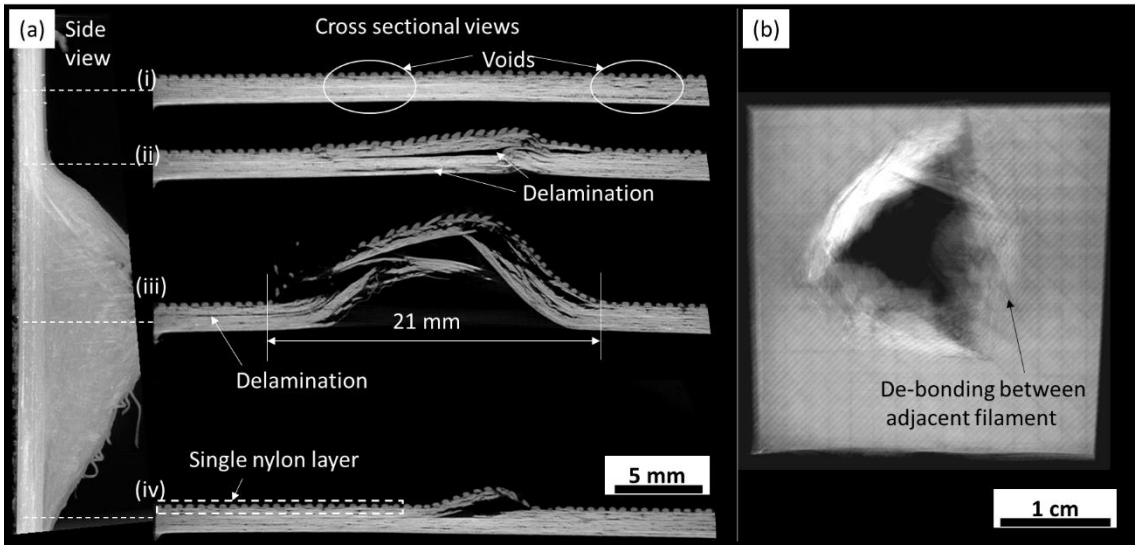

Figure 12 (a) CT-scan image of the side view and cross-sectional views of the fractured area of carbon fiber specimen (b) 3D view of the μCT-scan image of the fractured area of carbon fiber specimen

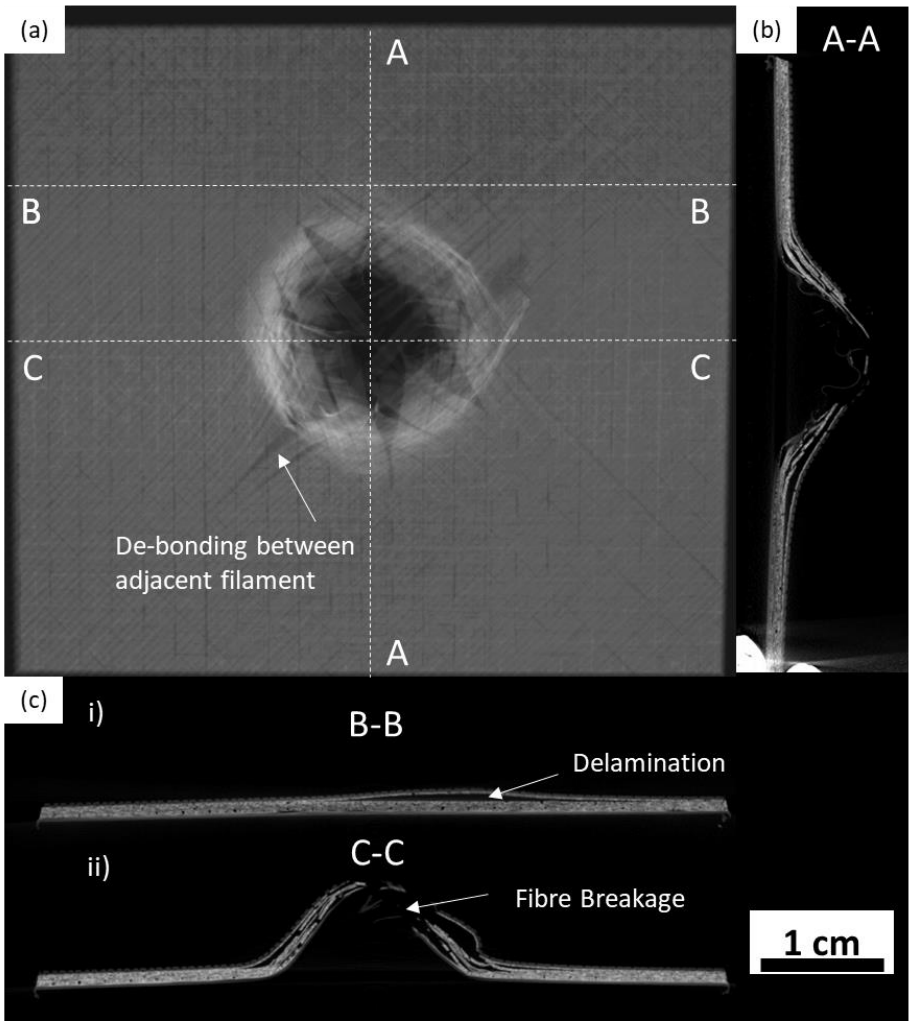

Figure 13 (a) Top view of the μCT-scan image of the fractured area of glass fiber specimen (b) CT-scan image of the side view of the fractured area of carbon fiber specimen (c) fiber specimen CT-scan image of the cross section view of the fractured area of carbon fiber specimen

4. Conclusion

Additively manufactured carbon and glass fibers reinforced thermoplastics are fabricated, characterized and reported in this paper. Mechanical tests such as tensile, flexural, and indentation tests are conducted and compared with the conventional CFRTP and GFRTP. The detailed fracture behaviors of the carbon and glass FRPs have been evaluated and discussed. Through this study, the potential and limitations of the process have been identified. The extrusion of pre-impregnated continuous carbon and glass fiber composites has enabled the

fabrication of high-performance structural parts owing to the high tensile strengths that the continuous fibers provide in comparison with other pure thermoplastics and short fiber reinforced thermoplastics. Unlike conventional composite manufacturing processes, the layer-by-layer laying of continuous fibers eliminates the need for expensive molds during the fabrication process making it ideal for prototyping and customization. However, additive manufacturing of continuous fiber reinforced thermoplastics is not going to replace the conventional composite manufacturing processes due to the low deposition rate of this technique. Having said that, the fabrication speed can be easily improved using multi-nozzle system. Instead of printing what has been done conventionally, this additive manufacturing technique of continuous fiber composite, on the other hand, complements the existing composite manufacturing processes by taking advantage of the complexity that AM enables to redesign composite parts. This study will be helpful to product designers wanting to attempt using FFF technique to fabricate continuous fiber composite parts.

Acknowledgement

This work was supported under the A*STAR TSRP – Industrial Additive Manufacturing Programme by the A*STAR Science & Engineering Research Council (SERC) [grant number 1325504105].

References

[1] G. Williams, R. Trask, I. Bond, A self-healing carbon fibre reinforced polymer for aerospace applications, Composites Part A: Applied Science and Manufacturing 38(6) (2007) 1525-1532.
[2] A. Mayyas, A. Qattawi, M. Omar, D. Shan, Design for sustainability in automotive industry: A comprehensive review, Renewable and Sustainable Energy Reviews 16(4) (2012) 1845-1862.
[3] H. Ullah, A.R. Harland, V.V. Silberschmidt, Dynamic bending behaviour of woven composites for sports products: Experiments and damage analysis, Materials & Design 88 (2015) 149-156.
[4] C.K. Chua, K.F. Leong, C.S. Lim, Rapid prototyping: principles and applications, World Scientific2010.
[5] V. Dikshit, A.P. Nagalingam, Y.L. Yap, S.L. Sing, W.Y. Yeong, J. Wei, Investigation of Quasi-Static Indentation Response of Inkjet Printed Sandwich Structures under Various Indenter Geometries, Materials 10(3) (2017) 290.

[6] V. Dikshit, Y.L. Yap, G.D. Goh, H. Yang, J.C. Lim, X. Qi, W.Y. Yeong, J. Wei, Investigation of out of plane compressive strength of 3D printed sandwich composites, IOP Conference Series: Materials Science and Engineering 139(1) (2016) 012017.
[7] Y.L. Yap, W.Y. Yeong, Shape recovery effect of 3D printed polymeric honeycomb, Virtual and Physical Prototyping 10(2) (2015) 91-99.
[8] G.D. Goh, S. Agarwala, G.L. Goh, V. Dikshit, S.L. Sing, W.Y. Yeong, Additive manufacturing in unmanned aerial vehicles (UAVs): Challenges and potential, Aerospace Science and Technology 63 (2017) 140-151.
[9] M.F. Afrose, S.H. Masood, P. Iovenitti, M. Nikzad, I. Sbarski, Effects of part build orientations on fatigue behaviour of FDM-processed PLA material, Progress in Additive Manufacturing (2015) 1-8.
[10] M.S. Wahab, K.W. Dalgarno, B. Cochrane, Synthesis of Polymer Nanocomposites for Selective Laser Sintering(SLS), Journal of Mechanics Engineering and Automation 1(2) (2011) 100-107.
[11] A. Sakly, S. Kenzari, D. Bonina, S. Corbel, V. Fournée, A novel quasicrystal-resin composite for stereolithography, Materials & Design 56 (2014) 280-285.
[12] H. Yang, J.C. Lim, Y. Liu, X. Qi, Y.L. Yap, V. Dikshit, W.Y. Yeong, J. Wei, Performance evaluation of ProJet multi-material jetting 3D printer, Virtual and Physical Prototyping 12(1) (2017) 95-103.
[13] U. Kalsoom, P.N. Nesterenko, B. Paull, Recent developments in 3D printable composite materials, RSC Advances 6(65) (2016) 60355-60371.
[14] E.P. Plueddemann, Interfaces in polymer matrix composites: Composite materials, Elsevier2016.
[15] N. Mohan, P. Senthil, S. Vinodh, N. Jayanth, A review on composite materials and process parameters optimisation for the fused deposition modelling process, Virtual and Physical Prototyping 12(1) (2017) 47-59.
[16] L.J. Love, V. Kunc, O. Rios, C.E. Duty, A.M. Elliott, B.K. Post, R.J. Smith, C.A. Blue, The importance of carbon fiber to polymer additive manufacturing, Journal of Materials Research 29(17) (2014) 1893-1898.
[17] H.L. Tekinalp, V. Kunc, G.M. Velez-Garcia, C.E. Duty, L.J. Love, A.K. Naskar, C.A. Blue, S. Ozcan, Highly oriented carbon fiber–polymer composites via additive manufacturing, Composites Science and Technology 105 (2014) 144-150.
[18] W. Zhong, F. Li, Z. Zhang, L. Song, Z. Li, Short fiber reinforced composites for fused deposition modeling, Materials Science and Engineering: A 301(2) (2001) 125-130.
[19] R.W. Gray IV, D.G. Baird, J. Helge Bøhn, Effects of processing conditions on short TLCP fiber reinforced FDM parts, Rapid Prototyping Journal 4(1) (1998) 14-25.
[20] R.W. Gray, D.G. Baird, J.H. Bøhn, Thermoplastic composites reinforced with long fiber thermotropic liquid crystalline polymers for fused deposition modeling, Polymer composites 19(4) (1998) 383-394.
[21] M.L. Shofner, K. Lozano, F.J. Rodríguez-Macías, E.V. Barrera, Nanofiber-reinforced polymers prepared by fused deposition modeling, Journal of applied polymer science 89(11) (2003) 3081-3090.
[22] M.L. Shofner, F.J. Rodríguez-Macías, R. Vaidyanathan, E.V. Barrera, Single wall nanotube and vapor grown carbon fiber reinforced polymers processed by extrusion freeform fabrication, Composites Part A: Applied Science and Manufacturing 34(12) (2003) 1207-1217.
[23] A. Plymill, R. Minneci, D.A. Greeley, J. Gritton, Graphene and carbon nanotube PLA composite feedstock development for fused deposition modeling, 2016. Available: http://trace.tennessee.edu/utk_chanhonoproj/1955/.

[24] S. Dul, L. Fambri, A. Pegoretti, Fused deposition modelling with ABS–graphene nanocomposites, Composites Part A: Applied Science and Manufacturing 85 (2016) 181-191.
[25] X. Wei, D. Li, W. Jiang, Z. Gu, X. Wang, Z. Zhang, Z. Sun, 3D printable graphene composite, Scientific reports 5 (2015).
[26] M. Nikzad, S.H. Masood, I. Sbarski, Thermo-mechanical properties of a highly filled polymeric composites for fused deposition modeling, Materials & Design 32(6) (2011) 3448-3456.
[27] S.H. Masood, W.Q. Song, Development of new metal/polymer materials for rapid tooling using fused deposition modelling, Materials & Design 25(7) (2004) 587-594.
[28] A. Gupta, A.A. Ogale, Dual curing of carbon fiber reinforced photoresins for rapid prototyping, Polymer composites 23(6) (2002) 1162-1170.
[29] A.A. Ogale, T. Renault, R.L. Dooley, A. Bagchi, C.C. Jara-Almonte, 3-D photolithography for composite development: discontinuous reinforcements, SAMPE quarterly 23(1) (1991) 28-38.
[30] R. Charan, T. Renault, A.A. Ogale, A. Bagchi, Automated fiber-reinforced composite prototypes, Fifth International Conference on Rapid Prototyping, 1994, pp. 91-97.
[31] N. Li, Y. Li, S. Liu, Rapid prototyping of continuous carbon fiber reinforced polylactic acid composites by 3D printing, Journal of Materials Processing Technology 238 (2016) 218-225.
[32] C. Yang, X. Tian, T. Liu, Y. Cao, D. Li, 3D printing for continuous fiber reinforced thermoplastic composites: mechanism and performance, Rapid Prototyping Journal 23(1) (2017. http://dx.doi.org/10.1108/RPJ-08-2015-0098).
[33] X. Tian, T. Liu, C. Yang, Q. Wang, D. Li, Interface and performance of 3D printed continuous carbon fiber reinforced PLA composites, Composites Part A: Applied Science and Manufacturing 88 (2016) 198-205.
[34] K. Mori, T. Maeno, Y. Nakagawa, Dieless forming of carbon fibre reinforced plastic parts using 3D printer, Procedia Engineering 81 (2014) 1595-1600.
[35] Y. Nakagawa, K. Mori, T. Maeno, 3D printing of carbon fibre-reinforced plastic parts, The International Journal of Advanced Manufacturing Technology 91(5-8) (2017. doi:10.1007/s00170-016-9891-7) 2811-2817.
[36] M. Namiki, M. Ueda, A. Todoroki, Y. Hirano, R. Matsuzaki, 3D printing of continuous fiber reinforced plastic, Proceedings of the Society of the Advancement of Material and Process Engineering, Seattle, WA, USA, 2014, pp. 1-6.
[37] W. Zhong, F. Li, Z. Zhang, L. Song, Z. Li, Research on rapid-prototyping/part manufacturing (RP&M) for the continuous fiber reinforced composite, Materials and Manufacturing Processes 16(1) (2001) 17-26.
[38] C. Yang, B. Wang, D. Li, X. Tian, Modelling and characterisation for the responsive performance of CF/PLA and CF/PEEK smart materials fabricated by 4D printing, Virtual and Physical Prototyping 12(1) (2017) 69-76.
[39] F. Ning, W. Cong, J. Qiu, J. Wei, S. Wang, Additive manufacturing of carbon fiber reinforced thermoplastic composites using fused deposition modeling, Composites Part B: Engineering 80 (2015) 369-378.
[40] Y. Wang, Mechanical properties of stitched multiaxial fabric reinforced composites from mannual layup process, Applied Composite Materials 9(2) (2002) 81-97.
[41] G.W. Melenka, B.K.O. Cheung, J.S. Schofield, M.R. Dawson, J.P. Carey, Evaluation and prediction of the tensile properties of continuous fiber-reinforced 3D printed structures, Composite Structures 153 (2016) 866-875.
[42] F. Van Der Klift, Y. Koga, A. Todoroki, M. Ueda, Y. Hirano, R. Matsuzaki, 3D printing of continuous carbon fibre reinforced thermo-plastic (CFRTP) tensile test specimens, Open Journal of Composite Materials 6(01) (2015) 18.

[43] J.M. Gardner, G. Sauti, J.W. Kim, R.J. Cano, R.A. Wincheski, C.J. Stelter, B.W. Grimsley, D.C. Working, E.J. Siochi, Additive manufacturing of multifunctional components using high density carbon nanotube yarn filaments, SAMPE 2016, Long Beach, CA, United States, 2016.
[44] J.M. Gardner, G. Sauti, J.-W. Kim, R.J. Cano, R.A. Wincheski, C.J. Stelter, B.W. Grimsley, D.C. Working, E.J. Siochi, 3-D printing of multifunctional carbon nanotube yarn reinforced components, Additive Manufacturing 12, Part A (2016) 38-44.
[45] R. Matsuzaki, M. Ueda, M. Namiki, T.K. Jeong, H. Asahara, K. Horiguchi, T. Nakamura, A. Todoroki, Y. Hirano, Three-dimensional printing of continuous-fiber composites by in-nozzle impregnation, Scientific reports 6 (2016).
[46] G.T. Mark, A.S. Gozdz, Three dimensional printer with composite filament fabrication, in: USPTO (Ed.) MARKFORGED, INC.

Somerville

MA, 2015.
[47] G.T. Mark, Methods for fiber reinforced additive manufacturing, in: USPTO (Ed.) Markforged, Inc, 2014.
[48] ASTM D3171-15 (Standard Test Methods for Constituent Content of Composite Materials), ASTM International, West Conshohocken, PA, 2015, www.astm.org.
[49] ASTM D3039 / D3039M-14, Standard Test Method for Tensile Properties of Polymer Matrix Composite Materials, ASTM International, West Conshohocken, PA, 2014, www.astm.org.
[50] ASTM D790-15e2, Standard Test Methods for Flexural Properties of Unreinforced and Reinforced Plastics and Electrical Insulating Materials, ASTM International, West Conshohocken, PA, 2015, www.astm.org.
[51] ASTM D6264 / D6264M-12, Standard Test Method for Measuring the Damage Resistance of a Fiber-Reinforced Polymer-Matrix Composite to a Concentrated Quasi-Static Indentation Force, ASTM International, West Conshohocken, PA, 2012, www.astm.org.
[52] E.C. Botelho, Ł. Figiel, M.C. Rezende, B. Lauke, Mechanical behavior of carbon fiber reinforced polyamide composites, Composites Science and Technology 63(13) (2003) 1843-1855.
[53] Sudarisman, I.J. Davies, The effect of processing parameters on the flexural properties of unidirectional carbon fibre-reinforced polymer (CFRP) composites, Materials Science and Engineering: A 498(1) (2008) 65-68.
[54] J. Sirichantra, S. Ogin, D. Jesson, The use of a controlled multiple quasi-static indentation test to characterise through-thickness penetration of composite panels, Composites Part B: Engineering 43(2) (2012) 655-662.
[55] I. Davies, H. Hamada, Flexural properties of a hybrid polymer matrix composite containing carbon and silicon carbide fibres, Advanced Composite Materials 10(1) (2001) 77-96.
[56] C. Weaver, J. Williams, Deformation of a carbon-epoxy composite under hydrostatic pressure, Journal of Materials Science 10(8) (1975) 1323-1333.

Figure Captions

Figure 1 Extrusion of pre-impregnated continuous fiber composite filament in FFF

Figure 2 Isotropic unidirectional fiber pattern (0 °) of a single layer. Fiber layers are stacked up on top of each other without any nesting.

Figure 3(a) SEM image of composite filament showing multi-strands of fibers (b) SEM image of a single raw carbon fiber composite filament (c) SEM image of the two overlapping extruded composite filaments (d) CT-scan image of cross section of composite specimen showing the voids formed between adjacent filament (e) Pore size distribution obtained from μCT-scan analysis

Figure 4 (a) continuous carbon fiber without observable breaking under optical microscope (b) breaking of carbon fibers at small turn radius (c) laser-optical image of multiple-strands of fibers at 50x magnification (d) laser-optical image of multiple-strands of fibers at 150x magnification

Figure 5 (a) Stress-strain curves of an additively manufactured carbon and glass FRTP (b) illustration of tensile fracture mechanism of additively manufactured FRTP (c) fracture mode that consists of cracking and delamination of a carbon fiber tensile specimen (d) fracture mode that consists of cracking and delamination of a glass fiber tensile specimen (e) matrix crack due to shear rupture and fiber breakage due to tensile rupture (f) SEM image showing fiber pull-out at the fractured surface (g) SEM image showing fiber breakage and matrix adhering to fiber

Figure 6 Typical 3-point bending test response of AM carbon and glass FRTP composite specimens

Figure 7(a) schematics illustrating fracture mode of carbon FRTP undergoing flexural test (b) fibers breakage occurred at the outer most layers which are in tensile (c) cross section view of the fracture surface (d) image sequence of the flexural test captured using high speed camera

Figure 8 (a) schematic showing the fracture modes of the additive manufactured glass FRTP undergoing flexural test (b) top view of glass fibers specimens with buckling of fibers (c) μCT image of the top view of the glass fibers specimen showing the shear kinking at the middle of the specimen (d) μCT image of the side view of glass fibers specimens showing the buckling of fibers at compressive layers

Figure 9 (a) μCT image of the side view of the glass fiber flexural test specimen undergone flexural test (b) cross sectional view of A-A (c) cut-out view of B-B showing shear kinking at top layer (d) cut-out view of C-C showing no obvious shear kinking at bottom layer

Figure 10 force-indentation curves for carbon and glass FRTPs

Figure 11(a) Deformation and delamination of fiber laminate before fiber breakage (b) fiber breakage of different fiber layup orientation after the indentation (c) failure mode of single fiber layup orientation which consists of fiber breakage and de-bonding between adjacent filament (d) cross section view which consists of delamination and fiber breakage in the indentation specimen

Figure 12 (a) CT-scan image of the side view of the fractured area of carbon fiber specimen

(b) 3D view of the μCT-scan image of the fractured area of carbon fiber specimen

Figure 13 (a) Top view of the μCT-scan image of the fractured area of glass fiber specimen (b) CT-scan image of the side view of the fractured area of carbon fiber specimen (c) fiber specimen CT-scan image of the cross section view of the fractured area of carbon fiber specimen

Tables

Table 1 Printing parameters

Table 2 Mechanical properties of FFF-fabricated CFRTP and GFRTP (average value ± standard deviation).

Figure 1

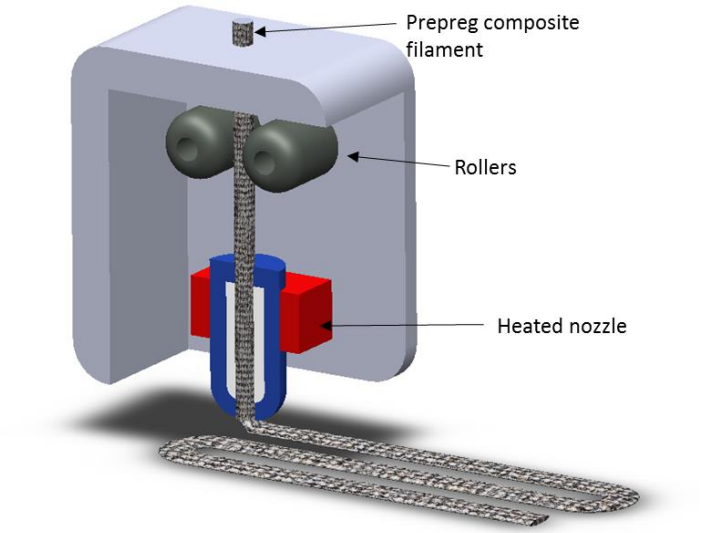

Figure 2

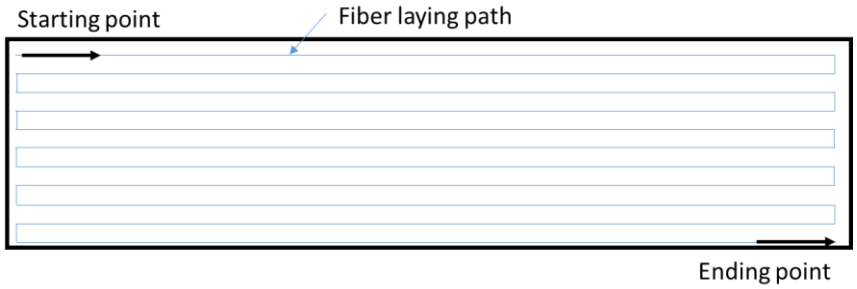

Figure 3

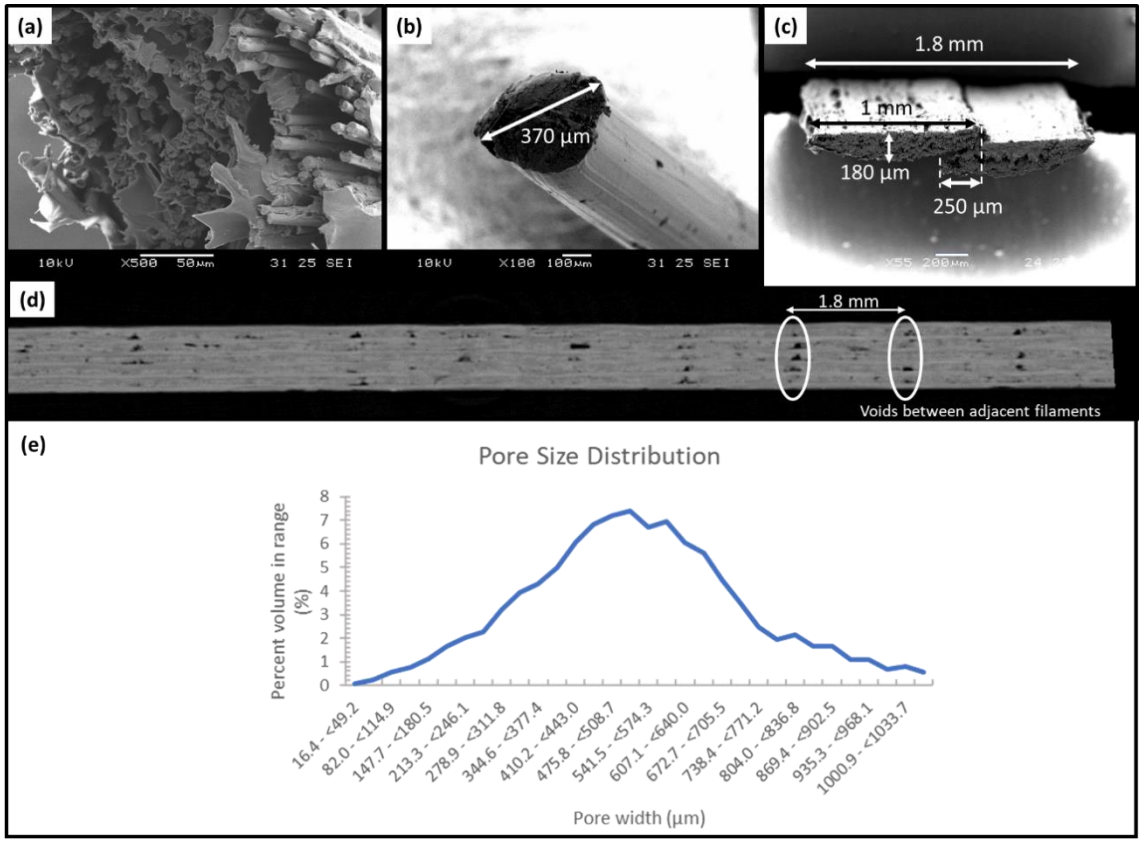

Figure 4

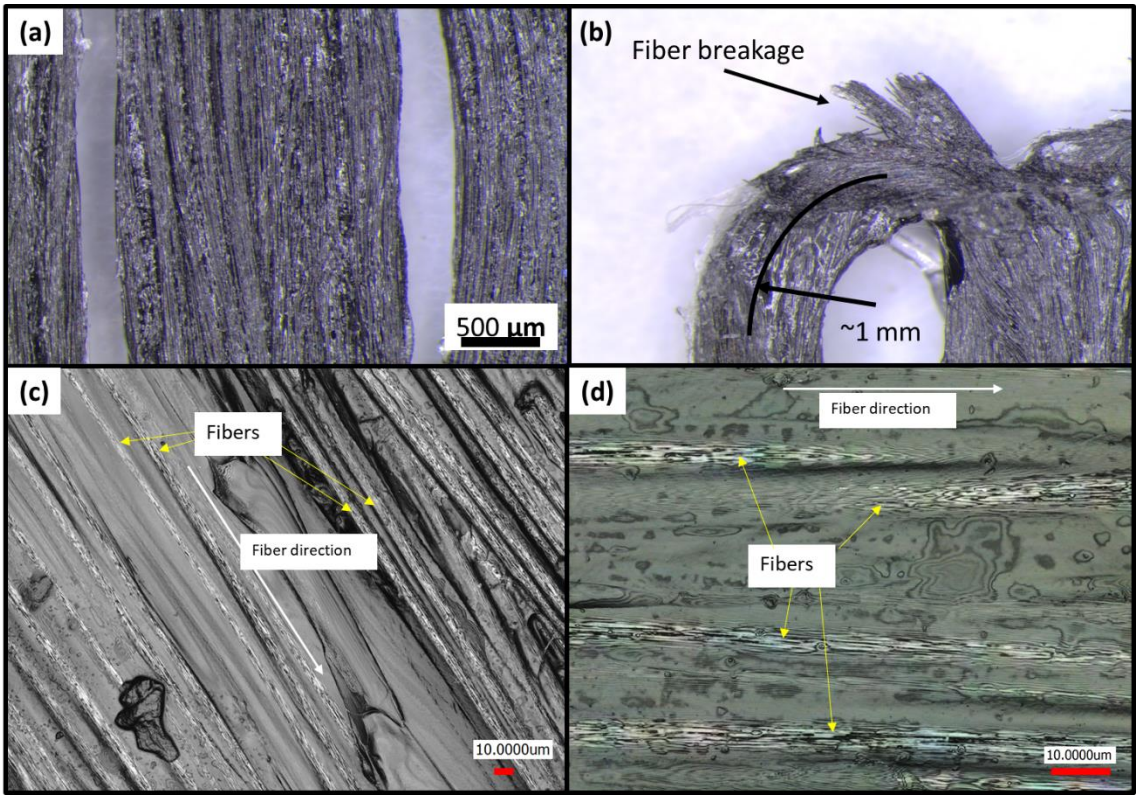

Figure 5

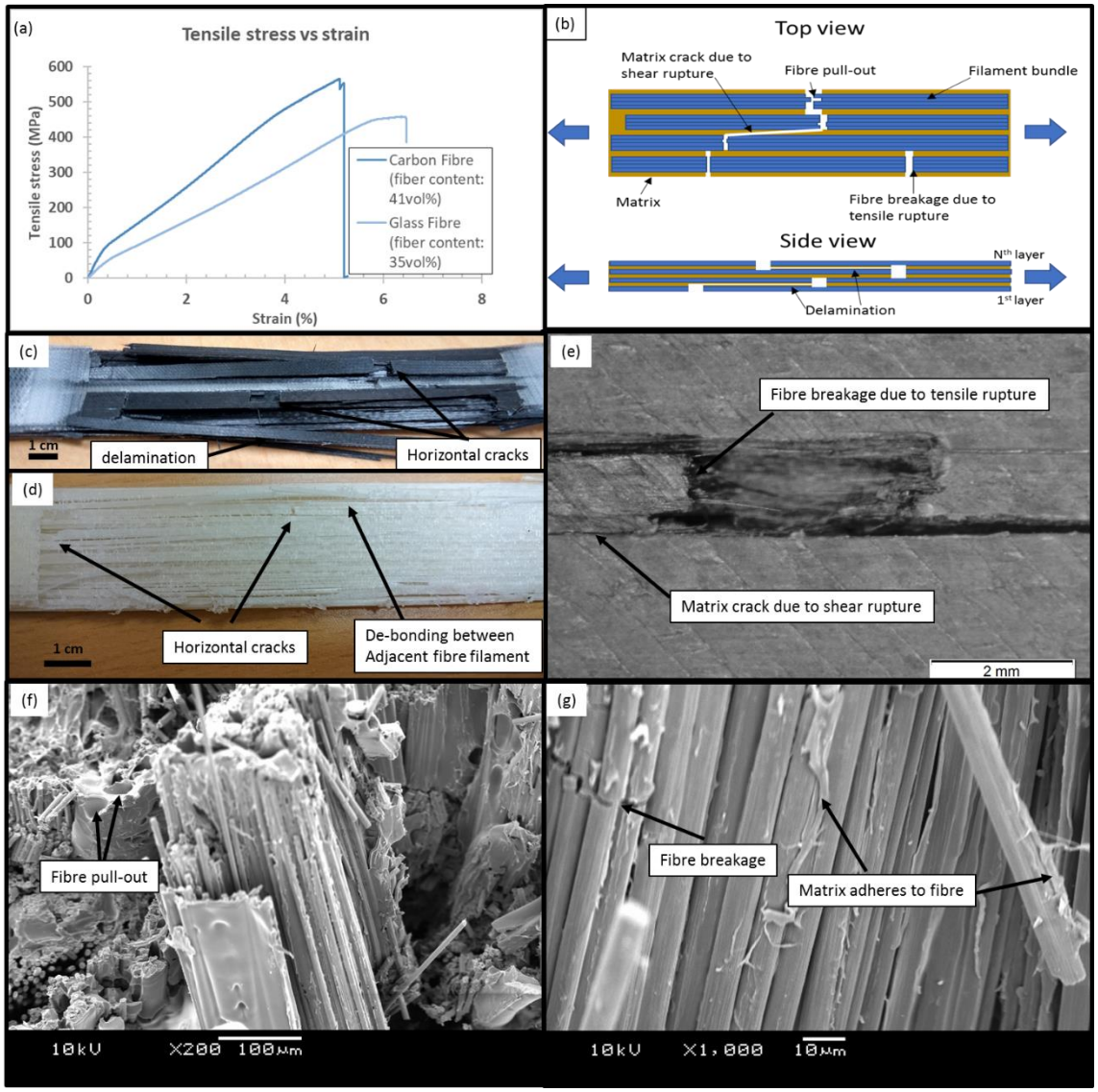

Figure 6

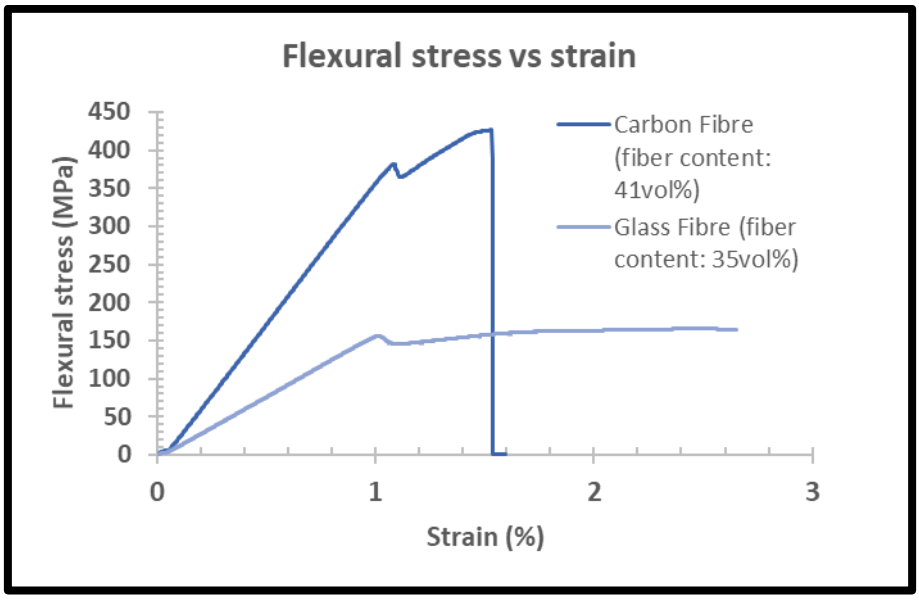

Figure 7

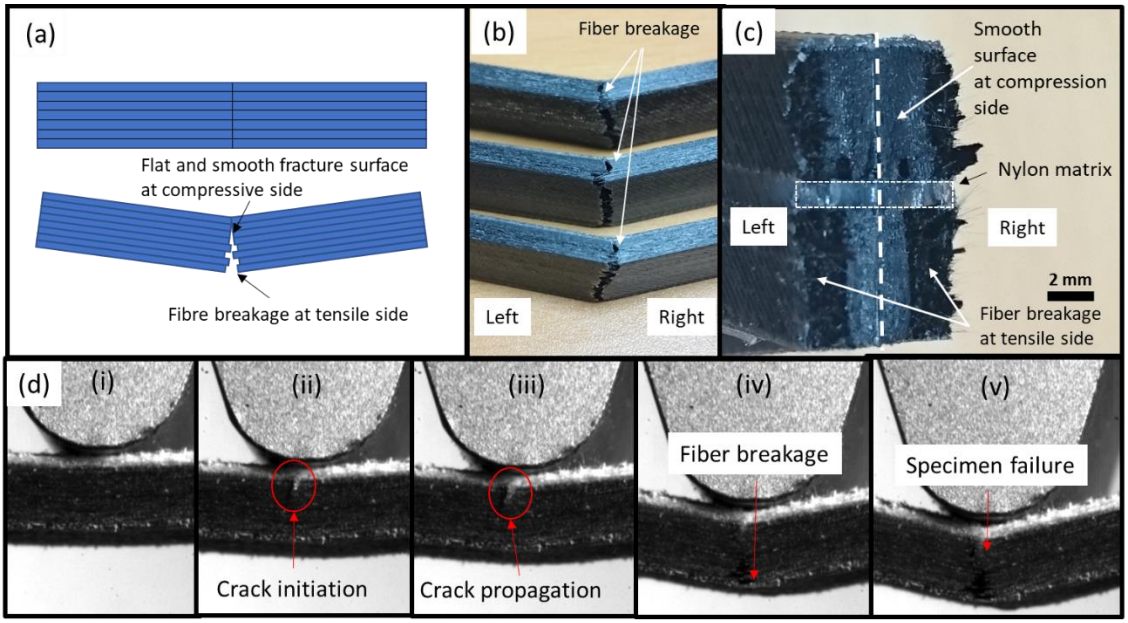

Figure 8

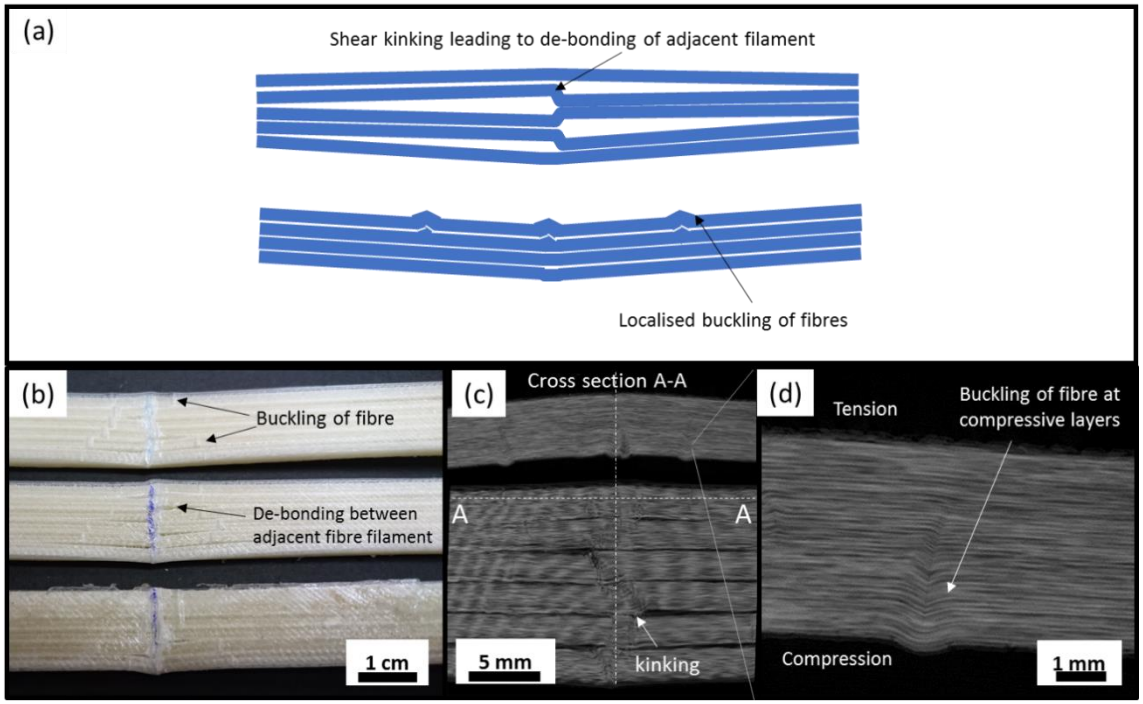

Figure 9

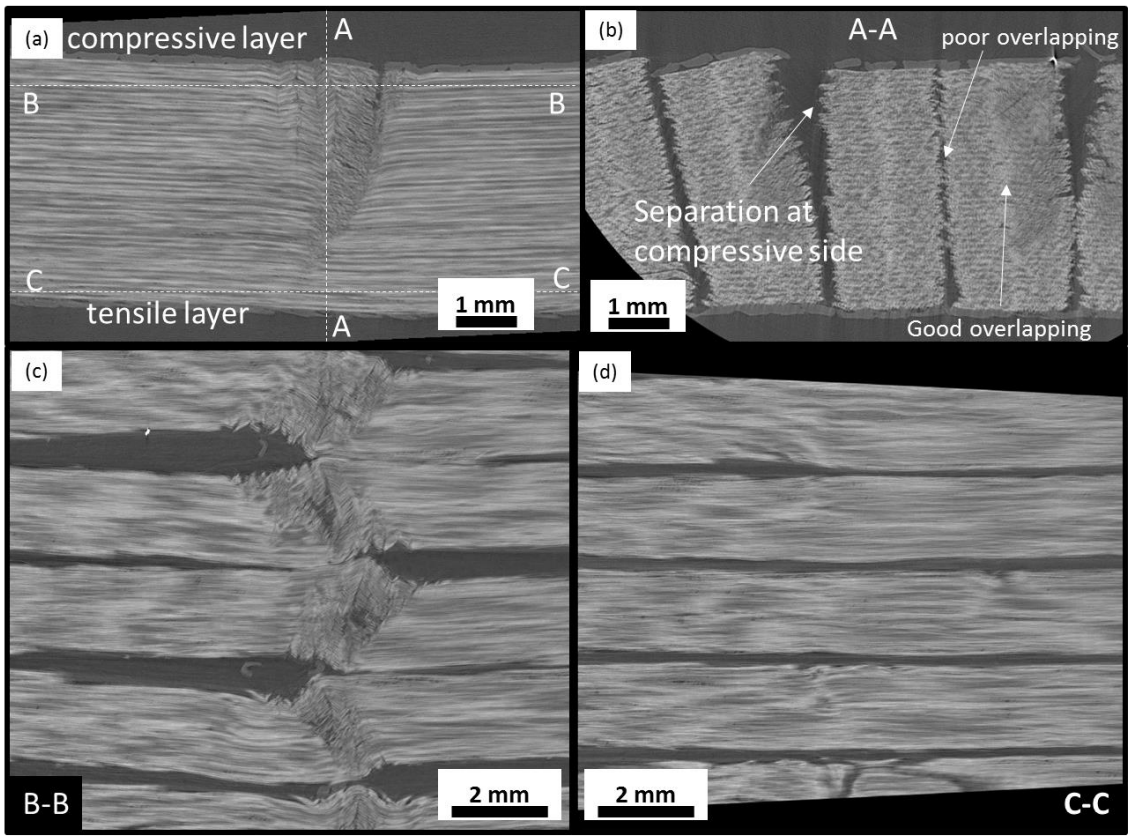

Figure 10

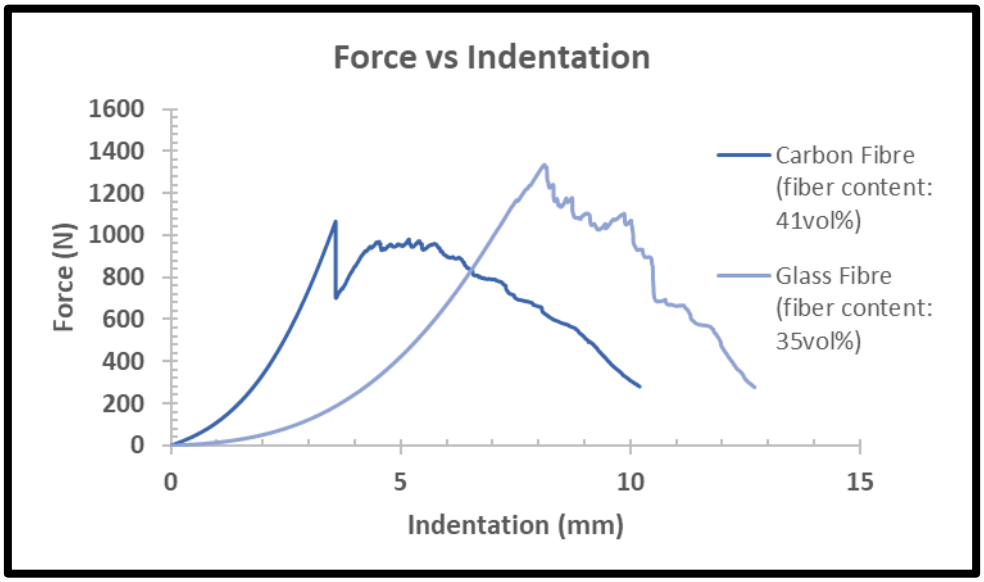

Figure 11

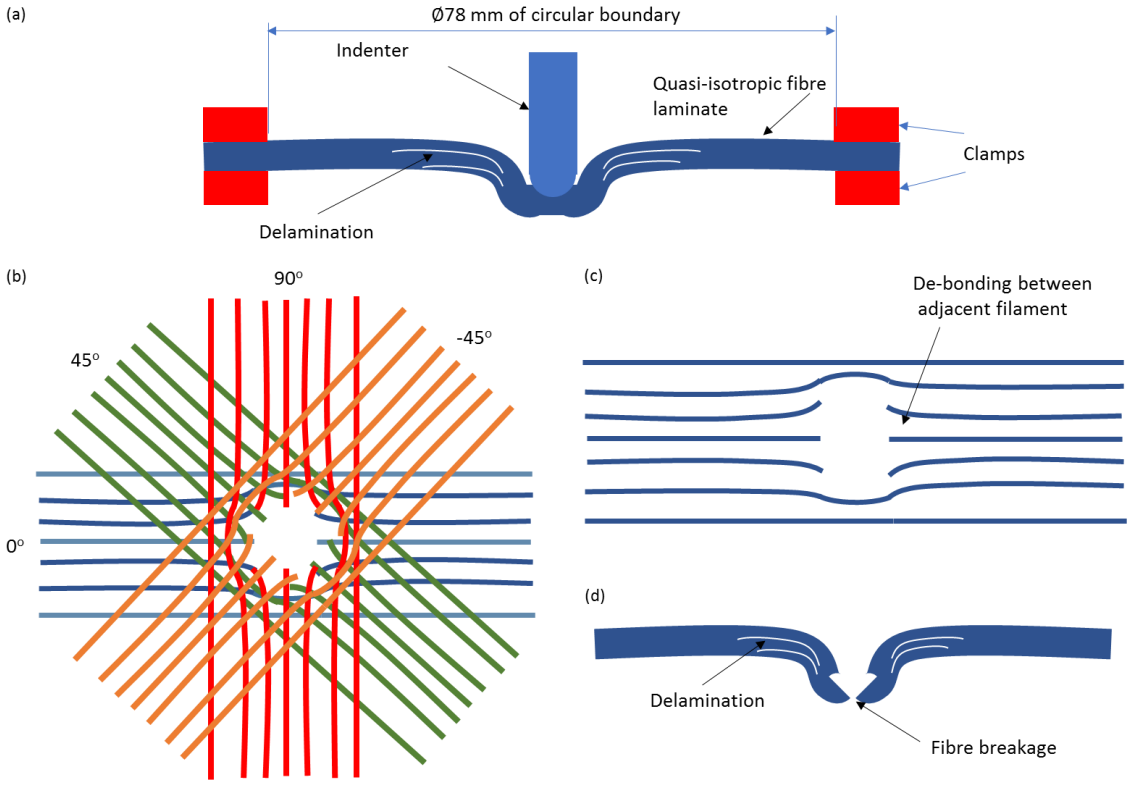

Figure 12

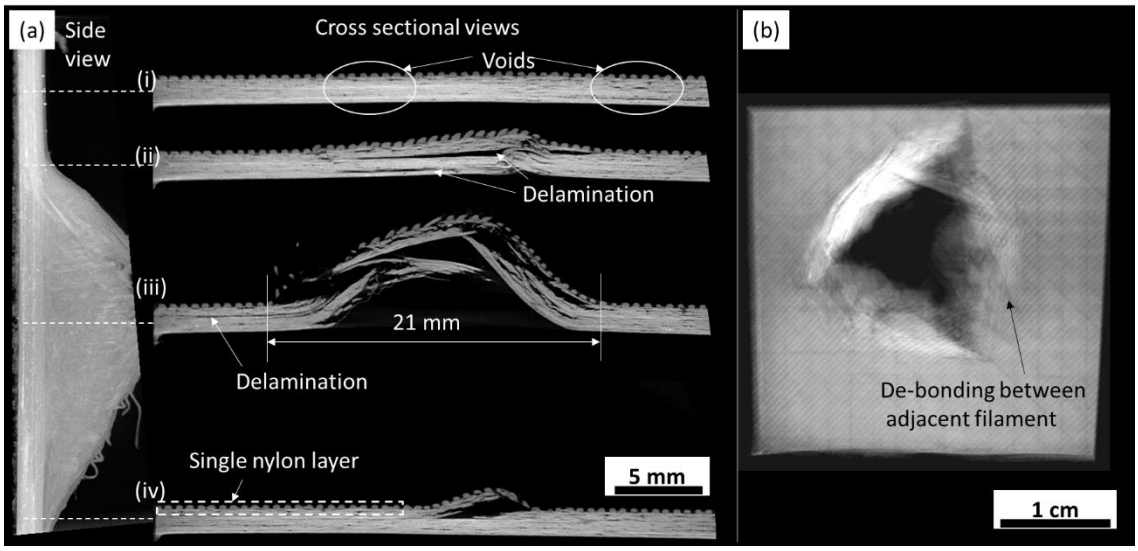

Figure 13

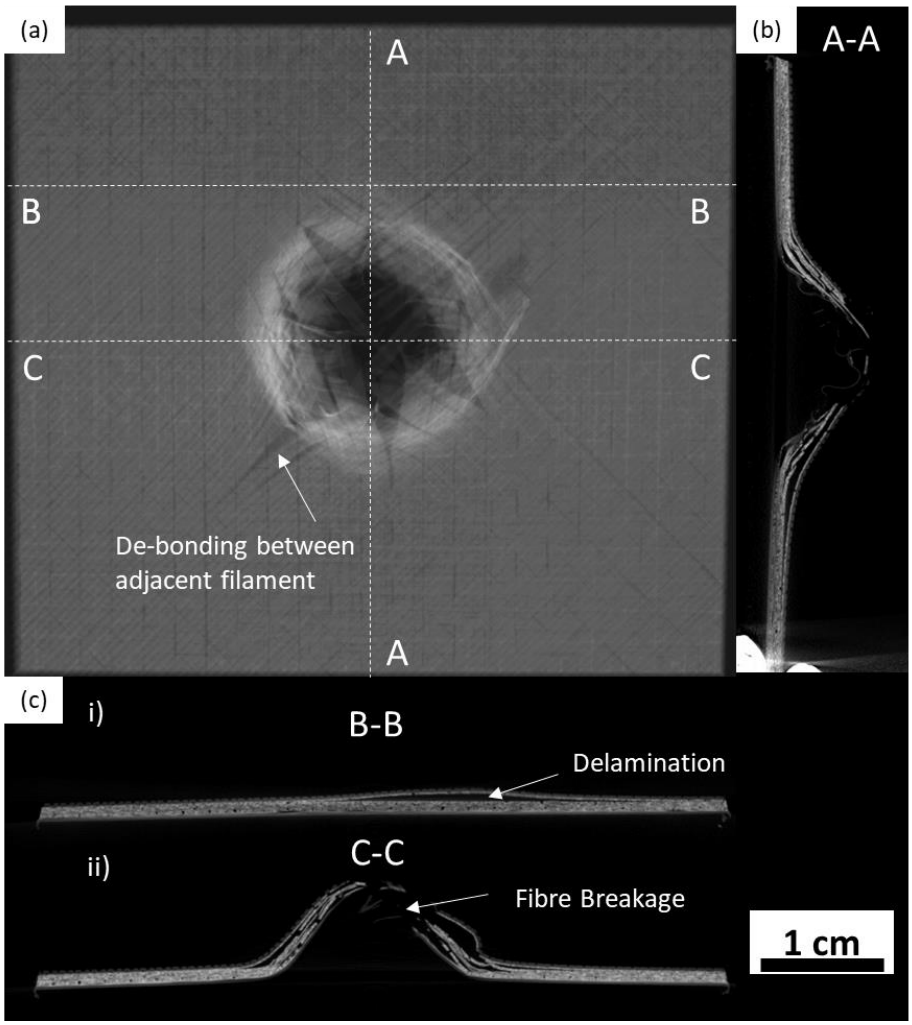

Table 1

Extruder temperature (°C)	Print pattern	Layer height (mm)	Infill (%)
260\	isotropic	0.1	100 (solid)

Table 2

		FFF GFRTP (V_f: 35_{vol}%)	Manufac-turer's data (GFRTP)	Conven-tional glass fiber composites	FFF CFRTP (V_f: 41_{vol}%)	Manufac-turer's data (CFRTP)	Conven-tional carbon fiber composites
Tensile test	Tensile Strength (MPa)	450 ± 1	590	225-235 [a]	600 ± 30	700	408[b]
	Young's Modulus (GPa)	7.20 ± 0.01	20	16.9-17.9 [a]	13.0 ± 1.0	50	71.4 [b]
Flexural test	Flexural Strength (MPa)	149± 10	310	356-359 [a]	430 ± 13	470	750[c]
	Flexural Modulus (GPa)	14.7±0.5	21	15-15.4 [a]	38.1 ± 1.0	48	47 [c]
Quasi-static Indentation test	Maximum Force, F_{max} (N)	1410 ±108	NA	NA	1080 ± 123	NA	1580[d]
	Displace-ment at maximum force (mm)	7.68 ± 0.43	NA	NA	3.54 ± 0.20	NA	NA
	Displace-ment @ 0.2*F_{max} (mm)	13.0 ± 1.0	NA	NA	10.6 ± 0.3	NA	NA
	Maximum Energy (J)	7050 ± 268	NA	NA	6260 ± 668	NA	NA

[a] V_f=38.3~41.5% E-glass stitched multi-axial non-crimp fabrics/epoxy composites[40]
[b] V_f=40% unidirectional carbon fabric/ PA 6/6 composites [52]
[c] V_f=47.5% unidirectional carbon fiber/epoxy composites [53]
[d] CFRP with a 0/90 configuration[54]